Table I Clinical phenotype and genotype of CGD patients at PGIMER Chandigarh

Family number	Patient	Clinical diagnosis	NBT or DHR122	Age at onset	Age at diagnosis	Follow up and prognosis	Gene involved (Protein encoded)	Exon/ Intron	Domain	Nucleotide change	Codon change
1	Patient 1	X-CGD	Both	1 month	2 years	1 year 8 months alive	CYBB (gp91phox)	Exon 4	Trans-memb domain III	271 C>T	p.Arg91X
2	Patient 2	X-CGD	NBT	10 days	7 months	7 days Dead	CYBB (gp91phox)	Exon 8	FAD binding domain	868 C>T	p.Arg290X
3	Patient 3	X-CGD	NBT	2 months	8 months	12 days Dead	CYBB (gp91phox)	Exon 5	Trans-memb domain IV	469 C>T	p.Arg157X
4	Patient 4	X-CGD	NBT	9 months	5 years	6 years alive	CYBB (gp91phox)	Exon 5	Extracellular domain	383 C>T	p.Gly145Arg
5	Patient 5	X-CGD	NBT	1 year	1 year	1 month Dead	CYBB (gp91phox)	Exon 11	NADP binding domain	1449 G>A	p.Trp483X
6	Patient 6	X-CGD	NBT	12 years	16 years	3 years 2 months alive	CYBB (gp91phox)	Exon 10	NADPH binding	1291 G>A	p.Ala431Thr
7	Patient 7	Presumed AR-CGD[a]	Both	1 1/2 months	2 years	2 months dead	CYBB, NCF-1, CYBA wild type	–	–	–	–
8	Patient 8	Presumed X-CGD[b]	NBT	3 months	9 months	1 month dead	N.D.	N.D.	N.D.	N.D.	N.D.
9	Patient 9	Presumed AR-CGD[a]	Both	5 months	1 year	1 years 6 months	CYBB, NCF-1, CYBA wild type	–	–	–	–
10	Patient 10	AR-CGD	NBT	10 months	10 years	3 years alive	NCF-1 (p47phox)	Exon 2	PX domain	73_74delGT	p.Tyr26HisfsX25
11	Patient 11	AR-CGD	Both	5 years	7 years	6 years alive	NCF 1 (p47phox)	Exon 2	PX domain	73_74delGT	p.Tyr26HisfsX25
12	Patient 12	AR-CGD	NBT	1 year	9 years	3 years alive	NCF-1 (p47phox)	Exon 2	PX domain	73_74delGT	p.Tyr26HisfsX25
13	Patient 13	AR-CGD	NBT	2 years	3 years	19 years alive	NCF 1 (p47phox)	Exon 2	PX domain	73_74delGT	p.Tyr26HisfsX25
13	Patient* 14	Presumed AR-CGD	NBT	5 years	9 years	5 years dead	N.D.	N.D.	N.D.	N.D.	N.D.
14	Patient 15	AR-CGD	Both	1 year 6 months	2 years	2 months alive	NCF-1 (p47phox)	Exon 2	PX domain	73_74delGT	p.Tyr26HisfsX25
14	Patient 16	AR-CGD	Both	2 years	4 years	2 months alive	NCF-1 (p47phox)	Exon 2	PX domain	73_74delGT	p.Tyr26HisfsX25
15	Patient 17	AR-CGD	DHR 123	4 months	3 years	4 years alive	NCF-1 (p47phox)	Exon 2	PX domain	73_74delGT	p.Tyr26HisfsX25

[a] Patients 8 and 10 were found to have no mutations in CYBB, CYBA and NCF-1

[b] Patient 9 has history of death of 3 elder male siblings *Patient 15 is the deceased sister of Patient 14

AR-CGD). One case had a history of loss of 3 elder male siblings and this was classified as presumed X-CGD. Two cases with no mutation in CYBB, NCF-1 and CYBA genes were presumed to be AR-CGD cases. The mean age for onset of symptoms was 1 year 8 months (median 10 months, range 1 month - 8 years) and a diagnosis of CGD was made at a mean age of 4 years 6 months (median 3.0 years, range 7 months -16 years). The mean age at diagnosis was significantly lower in children diagnosed with X-linked CGD compared those with autosomal recessive disease: mean 3 years 8 1/2 months (median 1 year, range 7 months–16 years) versus mean 5 years (median 3 years 6 months, range 1 year–10 years) respectively. Similarly the age at onset of symptoms was also different in two groups mean 2 years ½months (median 3 months, range 1 month–12 years) versus mean 1 year 10 months (median 1 year 3 months, range 1 1/2 months–5 years) (Table II).

Infectious Complications

All patients in the present cohort received prophylactic antimicrobials in the form of co-trimoxazole and Itraconazole or Ketoconazole after diagnosis. None of the patients received therapy with recombinant IFN-γ, because of financial constraints. Infectious episodes were managed with appropriate antimicrobials and antifungal agents including the newer antifungal agents such as voriconazole often for prolonged periods.

Pneumonia and recurrent lymphadenitis were the commonest clinical manifestations, present in 82.3 % (14/17) (Figure 1 and Table III). Recurrent skin and/or subcutaneous abscesses were found in 47 % (8/17) children. Hepatomegaly was detected in 59 % (10/17). In addition, liver abscesses were observed in 23.5 % (4/17) of children, in the absence of significant hepatomegaly in two children. Gastrointestinal symptoms in the form of loose stools, abdominal pain and distention were present in 35 % (6/17). Septicemia was detected in 25 % (4/16) children, albeit pre-terminally in 3 children. Bone and joint involvement was detected in 3 children. Perianal/ischiorectal abscess was also seen in 2 children. Other less common manifestations included recurrent otitis media and renal involvement, found in two children and one child respectively . Recurrent ulcerative stomatitis was also observed in one child (Table III).

Microorganims Isolated From Patients

An infectious etiology could not be established in most infectious episodes. Culture reports were often negative despite repeated blood and urine culture, culture of bronchoalveolar lavage whenever required on clinical grounds, fine needle aspirates and biopsy specimens probably because most of these children had received antimicrobials, including antifungals in some cases, prior to culture. Polymerase chain reaction based tests were not performed for etiological diagnosis because of lack of availability of the same. Aspergillus species was the most frequently isolated microorganism, being isolated from lung, synovium and blood in 6 patients. Apart from the common species i.e. *A fumigatus*, *A flavus,* some rarer species such as *A terreus* were also isolated. Candida species were also isolated in a significant proportion of cases (3/17). Fungal serology for *Aspergillus* was positive in four children (Table IV).

Staphyloccocus aureus was isolated from culture of pus in Patient 6 who preented with recurrent and multiple liver abscesses. *Burkholderia cepacia* was isolated from blood culture in one child with fulminant septicemia (Patient 2) and in one case *Mucor* was identified along with *Mycobacterium tuberculosis* from a resected segment of lung (Figure 2) (Patient 5). In addition *Fusarium dimerum* was cultured from the sputum in a child with autosomal recessive form of disease (Patient 16).

Table II Clinical course of children with CGD at PGIMER

	Overall (months/year)	X-linked CGD (months/year)	Autosomal recessive CGD (months/year)
Median age at onset (Range)	10 months (1 month–8 years)	3 months (1 month–12 years)	1 year 3 months (1 1/2 months–5 years)
Mean age of onset of symptoms (Mean ± SD)	1 year 8 months±2.4	2 years 1/2 months±4.4	1 years 10 months±1.8
Median age at diagnosis (Range)	3 years (7 months–16 years)	1 year (7 months–16 years)	3 years 6 months (1–10 years)
Mean age at diagnosis (Mean ± SD)	4 years 6 months±4.6	3 years 8 1/2 months±5.6	5 years±3.4
Mean delay in diagnosis (Mean ± SD)	2 years 10 months±2.9	1 year 8 months±1.8	3 years 2 months±3.0
Median delay in diagnosis	2 years (0–9 years 2 months)	6 months (0–4 years 3 months)	2 years (6 months–9 years 2 months)
Deceased	6/17 (35 %)	4/7 (57 %)	2/10 (20 %)
Median age at death (Range)	1 year 5 months (7 months–14 years)	10 months (7 months–2 years)	9 years

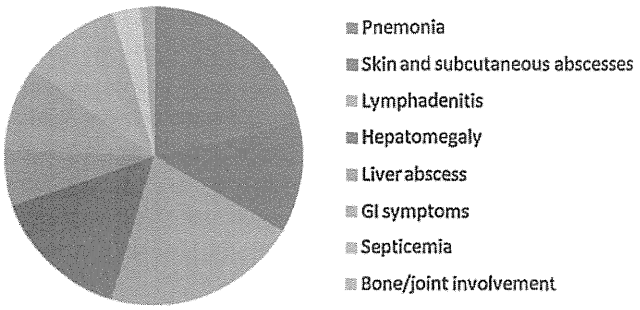

Fig. 1 Predominant clinical manifestations in children with CGD

Non Infectious Complications

Two X-CGD patients presented with abdominal pain and distention without any evidence of an infectious etiology. Patient 8 presented with features of intestinal obstruction with abdominal distention and pain. This was initially attributed to sepsis, the antimicrobials were changed twice. However when he did not respond to this regimen, steroids were given to which he responded dramatically with improvement in the gastrointestinal symptoms. However subsequently he developed respiratory distress and succumbed to his illness.

Patient 1 with X-linked form of the disease presented with fever, hepatosplenomegaly and persistent anemia, thrombocytopenia, hyperferritinemia (1,013 ng/ml) and mild hypertriglyceridemia (301 mg/dl) on follow-up. Bone marrow examination showed evidence of hemophagocytosis. His fibrinogen level was however normal at 2.4 g/l. A diagnosis of hemophagocytic lymphohistiocytosis (HLH) was made based on the clinical features and laboratory parameters. He responded well to immunosuppressive therapy in combination with intravenous vancomycin, meripenem and voriconazole.

Patient 4 presented with renal involvement in the form of mildly deranged renal function tests and hydronephrotic changes in the right kidney.

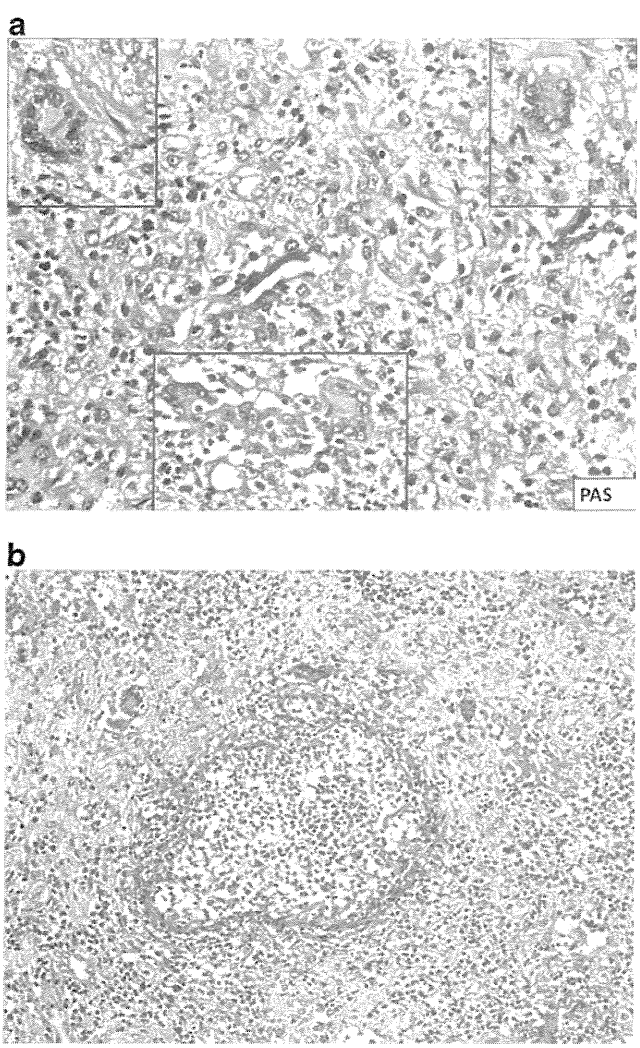

Fig. 2 **a** Photomicrograph showing epithelioid granulomas with multinucleate giant cells. **b** Photomicrograph depicting angioinvasion (H&E) ×40

Table III Infectious complications in the patients

Site of disease	No. of patients (%)	No of episodes	No of patients with ≥1 episode	% of patients with ≥1 episode
Lung	14 (82.3 %)	40	12	71 %
Skin/subcutis	8 (47 %)	28	8	47 %
Lymph node	14 (82.3 %)	32	11	65 %
Gastrointestinal	4 (23.5 %)	10	3	18 %
Liver	4 (23.5 %)	11	2	12 %
Kidney/Urinary Tract	1 (6 %)	1	0	0 %
Septicemia	4 (23.5 %)	6	2	12 %
Ear	2 (11.8 %)	4	2	12 %
Bone/Joint	3 (11.8 %)	5	2	12 %

Investigations

Most of the children had panhypergammaglobulinemia with mean IgG level of 1571.5±450 g/dl, mean IgM level

Table IV Microorganisms isolated from the patients

Microorganisms	Number of patients	Percentage
Staph aureus	2	12
Aspergillus flavus	3	18
Aspergillus fumigatus	2	12
Aspergillus terreus	1	6
Burkholderia cepacia	1	6
Mucor	1	6
Mycobacterium tuberculosis	1	6
Fusarium dimerum	1	6
Candida sp.	3	18

of 232.9 ±101.2 g/dl and a mean IgA level of 252.8± 179 g/dl. Lymphocyte subsets were within normal range in most children.

Nitroblue Dye Reduction Test [8, 9]

Leucocyte rich plasma was separated from heparin anticoagulated blood from both test and control subjects. Two drops (100 μl) each of leucocyte rich plasma was placed on 2 different glass slides labeled as "stimulated" and "unstimulated" respectively. Two drops of (100 μl) of a 0.2 % Nitroblue tetrazolium dye was added to each slide. One drop of a 20 % suspension of Baker's yeast was added to the slide labeled as "stimulated". Both the slides were then placed in a humified chamber at 37 °C for 30 min. The slides were taken out after 30 min, cover slips were placed on both them and they were examined under a light microscope.

Neutrophils showing blue black cytoplasmic clumps of formazan were counted in both stimulated and unstimulated tests. At least 100 neutrophils were counted and the results were expressed as a percentage of cells showing the blue black granules. The procedure was repeated similarly with the control sample. Normally 85–95 % of stimulated neutrophils showed reduction of nitroblue tetrazolium to blue black formazan. Tests in which less than 30 % of stimulated neutrophils showed no reduction were interpreted as abnormally low and suggestive of chronic granulomatous disease. In some cases 2 μl of (100 μg/ml) of Phorbol myristate acetate was used to stimulate the neutrophils.

Dihydrorhodamine Assay [10, 11]

Staining Procedure

Four tubes, two each for normal control and patient sample were labeled as unstimulated and stimulated. Hundred (100 μl) of heparin anticoagulated blood was added to each tube. 1 μl of 1 mM Dihydrorhodamine (Sigma Cat No D1054) in DMSO was added to each tube and incubated for 15 min at 37^0C in a water bath. 2 μl of Phorbol-12- myristate-13- acetate (100 μg/ml) was added to the tubes labeled stimulated for both test and control samples. The tubes were further incubated for further 15 min at 37^0C and then lysed using BD FACS lysing solution for 10 min. The tubes were then centrifuged at 1,500 rpm for 5 min. Wash the cells with Phosphate buffered saline and spun again at 1,500 rpm for 5 min and decant supernatant. This procedure was repeated twice.

Acquisition and Data Analysis

Samples were acquired on FACS Calibur or FACS CANTO flow cytometer. Threshold was adjusted to exclude debris and neutrophils were gated by Forward Scatter(FSC)/Side scatter (SSC) gating. At least 10,000 gated events were acquired and recorded for each tube. Mean fluorescence intensities (MFIs) of stimulated and unstimulated samples and fold change in MFIs for both test and control samples was recorded.

Interpretation

The assay was performed in 7/17 patients. Four (4) of these patients were AR-CGD cases with a mutation in NCF-1 gene. Two of these were presumed AR-CGD (Patient 7 and 9) and one patient was a case of X-CGD with a mutation in the CYBB gene. The mean of mean fluorescence intensities in the unstimulated state in test was 52.6±59.2 and in the stimulated state was 68.9±78 and mean fold change was 1.23± 0.2. In the control the mean MFI in the unstimulated tube was 39.82±52 and in the stimulated tube was 627. 16±880 and the mean fold change was 21.75±18.1 A diagnosis of CGD was considered when there was no shift in the histograms after stimulation with PMA and minimal or no change in MFIs in unstimulated vs stimulated states (Table V) (Fig. 3a–d).

We could not estimate resdiual NADPH oxidase activity as superoxide production was not estimated in any of the cases.

Molecular Basis of the Defects

Molecular defects could be identified in 13 of the 17 patients with CGD. The mutation analysis could not done in 4 cases because some of the children were diagnosed when facilities for mutation studies were not available or the children had died before these studies could be performed. A mutation in the *CYBB* gene was detected in 6 children with X-linked CGD in which the mutation analysis was performed. All the six mutations detected in the CYBB gene were point mutations. Four of these six point mutations were nonsense mutations and 2 were missense mutations. The two missense mutations in the *CYBB* gene were novel and both mutations were deleterious using the SIFT program for the prediction of protein change. Same type of mutation in *NCF1* gene encoding for *p47phox* protein (c. 73_74delGT, p.Tyr26HisfsX25) were detected in 7 of the 8 children with AR- CGD in whom mutation analysis was performed (Table I).

Mortality and Cause of Death

Six of the 17 patients (35 %) had succumbed at the time of the analysis. Four of these were boys who had X-linked CGD (Patients 2, 3, 5, and 8) and Patient 15 who was a sister of

Table V Details of dihydrorhodamine assay in patients with CGD at PGIMER

Patient	MFI unstim pt	MFI stim pt	Fold change [SI]	MFI unstim cont	MFI stim cont	Fold change [SI] cont
Patient 1	8.5	8.69	1.02	7.79	174.1	22.35
Patient 7	11.25	12.7	1.12	23	380.91	16.56
Patient 9	8.8	9.9	1.12	2.8	173	61.78
Patient 11	175	223	1.8	155	2612	16.85
Patient 15	37.46	50.29	1.34	28.82	301.7	10.47
Patient 16	59.98	62.44	1.04	28.82	301.7	10.47
Patient 17	67.34	114.98	1.7	32.51	446.72	13.74
Mean ± SD	52.6±59.2	68.9±78	1.23±0.2	39.82±52	627. 16±880	21.75±18.1

MFI unstim pt: Mean fluorescence intensity unstimulated patient, MFI stim pt: Mean fluorescence intensity stimulated (PMA) patient

MFI unstim cont: Mean fluorescence intensity unstimulated control, MFI stim pt: Mean fluorescence intensity stimulated (PMA) control, SI : Stimulation index

patient 14 with AR-CGD with mutation in *NCF1* gene had also died. Patient 7 with presumed AR-CGD had also succumbed to his illness at time of analysis. Median age at death was 1 year 5 months with a range of 7 months–9 years. The median age at death in children with XL-CGD was 10 months with a range of 7 months–2 years. Three children

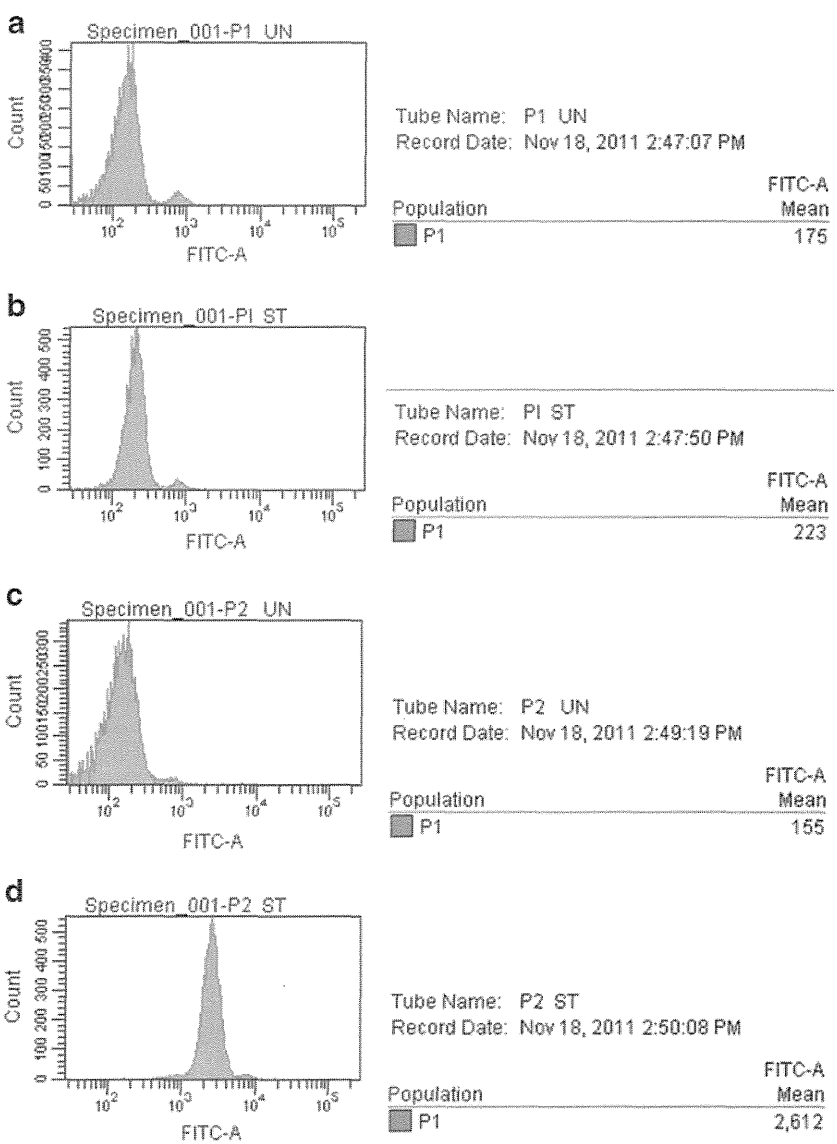

Fig. 3 Histograms from a DHR assay showing MFIs in gated neutrophils (**a**) Unstimulated patient (**b**) Post stimulation with PMA patient (**c**) Unstimulated normal control (**d**) Post stimulation with PMA normal control

with X-linked CGD died of fulminant septicemia. Another child (Patient 5) with X-linked CGD died of a massive pulmonary bleed following decortication to remove a segment of the lung for Mucormycosis. One girl (Patient 15) with autosomal recessive CGD and another child with presumed AR-CGD (Patient 7) died due to fulminant pneumonia at the age of 14 years and 2 years respectively. Mean survival in X-CGD was estimated to be 31.23 months (95 % CI: 5.1, 57.8 months) while the mean survival in AR-CGD was 176.6 months (95 % CI : 72.2, 281 months). This difference in survival was found to be close to level of statistical significance by Log Rank (Mantel-Cox) test ($p=0.065$) (Fig. 4).

Discussion

Chronic granulomatous disease has been infrequently been reported from India with only occasional case reports [12–15]. However in these case reports a presumptive diagnosis of CGD was made on the basis of NBT dye reduction test without a confirmed diagnosis by genetic analysis. The present study is to best of our knowledge the largest case series of CGD from India with a well-characterized molecular defect in 13 of the 17 patients. Thirteen cases of CGD have been reported from another tertiary care centre in North India in a period of 2 years between July 2004–August 2006 [16]. However all the cases in this study where diagnosed on the basis of NBT dye reduction test, DHR assay was not performed and the diagnosis was not confirmed by a genetic analysis for the putative genes in CGD in any of these patients.

AR-CGD was more common in the present series detected in 58 % of children compared to X-linked form of disease which was detected in 42 % of children. This is in contrast to previous studies from Europe and USA in which X-CGD. [1, 17, 18] and similar to a large series reported from Turkey [19] and another series from Tunisia [20]. Consanguinity is not frequent in North India as has been reported from the series reported from Turkey and Tunisia. Consanguinity was found in 2/17 patients in our cohort and both had AR-CGD with mutation in the NCF-1 gene. However the pattern of marriages is largely endogamous, with marriages being restricted within closed knit communities and this may result in a higher incidence of different autosomal recessive diseases in different population groups [21]. The mean age at diagnosis was 4 years 6 months whereas the mean age of onset of symptoms was 1 year 8 months and children with X-linked CGD were diagnosed earlier than AR- CGD, similar to cohorts reported earlier[22, 23]. Clinical manifestations were also similar to what has been reported earlier with rare and interesting findings in two cases [22–24].

Hemophagocytic lymphohistiocytosis (HLH) is a rare and potentially fatal complication of CGD. Only few cases of HLH complicating the course in CGD have been reported thus far. Apart from an increased susceptibility to recurrent infections by intracellular microorganisms, CGD is also associated with hyperinflammation and proinflammatory cytokine milieu, which could predispose these children to HLH. Most cases of HLH in children with CGD are secondary to infections mainly with Burkholderia cepacia and Leishmania. An isolated case with a perforin gene variant has also been reported [25–27].

One of the children had pulmonary mucormycosis (Fig. 2a and b) along with a co-infection with *Mycobacterium tuberculosis*. This child presented with a mass in the right hemithorax eroding the ribs and extending into the mediastinum. Mucormycosis has rarely been reported in patients with CGD, almost exclusively in those receiving prolonged and significant immunosuppression [26, 27]. However this child had not received any form of immunosuppressive therapy,

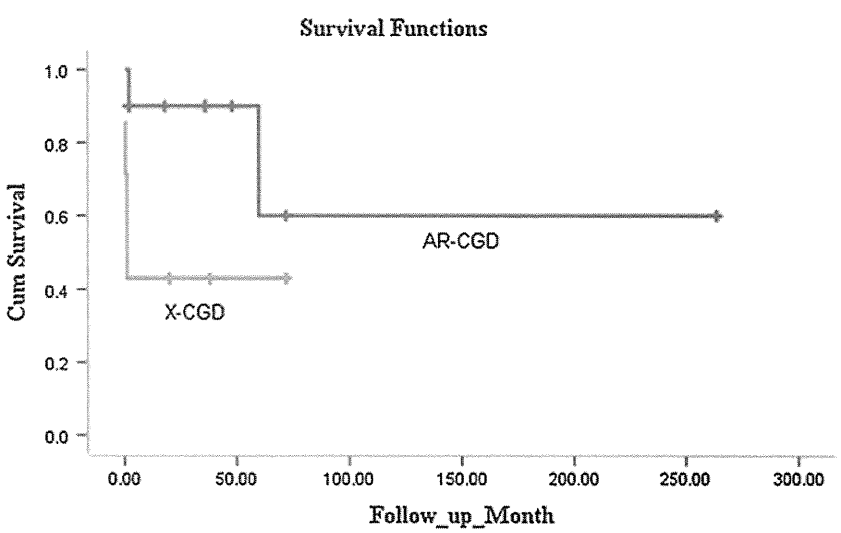

Fig. 4 Survival and follow-up in AR-CGD vs X-CGD

highlighting that mucormycosis can occur in CGD even without immunosuppression.

Mycobacterial infections both due to BCG and M. tuberculosis have been reported in patients with CGD from China, Iran and Latin America [28, 29]. Mycobacterium was detected in only one of our patients, diagnosed by detection of acid fast bacilli in a lung biopsy specimen. Although BCG vaccine is administered at birth in India only one child in our cohort developed suppuration at site of BCG administration followed by swelling at the root of the neck. The apparently low incidence of BCG and Mycobacterium tuberculosis infection in our cohort of CGD patients could be due to under detection. Moreover, some of the children presenting pneumonic consolidation did receive antitubercular therapy based on a presumptive diagnosis of tuberculosis. Two children in our cohort were diagnosed as tuberculosis based on the finding of granulomatous inflammation in lung biopsy specimens despite no isolation of Mycobacterium on culture or demonstration of acid-fast bacilli in the biopsy specimens. Recently germline mutations in the *CYBB* gene that selectively impair the activity of the NADPH oxidase complex in the monocyte-derived macrophages but not monocytes and neutrophils and predisposition to infection by *Mycobacteria tuberculosis* have been reported [30].

The spectrum of microorganisms isolated in the present series were similar to those reported in earlier studies [24, 31, 32]. Aspergillus was the most common organism isolated in our cohort followed by Staphylococcus *aureus*, Burkholderia *cepacia* and Candida. Several previous studies have shown that Aspergillus is emerging as the single most significant pathogen for infectious complications and mortality in patients with CGD. In North America, majority of infections in CGD are caused by five microorganisms namely *Staphylococcus aureus*, Burkholderia cepacia, *Serratia marcescens*, Nocardia and Aspergillus species [1].

All the presently known mutations in the *CYBB* gene have been reported in a large series recently [33]. It comprised of 1,267 unrelated kindreds with 1,415 patients. Six hundred and eighty one different mutations were identified in the patients and 487 (73.1 %) of these mutations were unique for one kindred. Single nucleotide substitutions were the commonest mutations reported. The missense mutations, splice site mutations and nonsense mutations were observed in 21.3 %, 17.6 % and 14.1 % respectively. Deletions contributed to 35.6 % of all mutations and insertions to 8 % of the mutations. All the mutations in *CYBB* gene in our cohort were single nucleotide substitutions; 66.7 % were nonsense mutations and 33.3 % were missense mutations. Two novel deleterious missense mutations were detected in our cohort.

Similarly a large series of all known mutations in the genes implicated in AR-CGD have also been published [34]. All the patients with AR- CGD in our cohort were found to have a same mutation in the *NCF1* gene encoding for *p47phox* protein although they were unrelated. Mutation in *NCF1* gene is the commonest cause of AR- CGD and accounts for approximately 20–25 % of all cases. All the patients also had the same mutation in the *NCF1* gene i.e. GT dinucleotide deletion in exon 2. This particular mutation has been reported in more than 60 patients worldwide with AR-CGD due to mutation in NCF1 gene and 97 % of the alleles [35]. There are 2 pseudo *NCF1* genes with a GT deletion in each of them. The preponderance of this mutation in patients can be explained by multiple recombination events between the functional *NCF1* gene and these closely linked pseudogenes, each gene having multiple recombination hot spots such as Alu repeats, Chi sequence and human mini-satellite repeats [36].

The overall mortality (35 %) was higher than what has been reported previously. The mortality in a large cohort of 429 patients from Europe was 20 % [23] whereas in an Italian cohort the mortality was 13 % [22]. This high mortality could be attributed to several factors. None of our patients received recombinant interferon γ. All patients were managed on cotrimoxazole and itraconazole prophylaxis along with management of breakthrough infections. The possibility of increased exposure to infectious agents in a developing, tropical country might have also contributed to a higher incidence of infections.

A higher frequency as well as greater severity of breakthrough infections compared to developed countries could have contributed to the increased mortality. Delay in initiating therapy for intercurrent infections due to the parents having to travel long distances to reach medical facilities and poor economic conditions are likely to have contributed significantly to this higher mortality. Haemotopoietic stem cell transplantation was not performed in any of our patients.

Finally although the total number of patients in the present cohort is very small to draw definite conclusions, it was observed that the course and outcome of the disease was much worse in children diagnosed with XL-CGD compared to AR forms of the disease. Four of the seven children (4/7) with X-CGD were dead at the time of data analysis. Three of these four children had nonsense mutations in the *CYBB* gene resulting in a stop codon as has been reported previously [1, 23, 29]. However it has also been conclusively shown that residual NADPH oxidase activity determined largely by the specific mutation in any of genes responsible for CGD rather than the gene itself is a useful predictor of outcome and survival [37]. It can also be concluded from this cohort that it is possible to provide a reasonable quality of life to patients with prophylactic antimicrobials even in a developing country like ours with all its constraints.

References

1. Winkelstein JA, Marino MC, Johnston Jr RB, Boyle J, Cumutte J, Gallin JI, et al. Chronic granulomatous disease. Report on a national registry of 368 patients. Medicine (Baltimore). 2000;79(3):155–69.
2. Janeway CACJ, Davidson M, Downey W, Gitlin D, Sullivan JC. Hypergammaglobulinemia associated with severe, recurrent, and chronic non-specific infection. Am J Dis Child. 1954;88:388–92.
3. Berendes H, Bridges RA, Good RA. A fatal granulomatosus of childhood: the clinical study of a new syndrome. Minn Med. 1957;40(5):309–12.
4. Bridges RA, Berendes H, Good RA. A fatal granulomatous disease of childhood; the clinical, pathological, and laboratory features of a new syndrome. Am J Dis Child. 1959;97(4):387–408.
5. Kuijpers T, Lutter R. Inflammation and repeated infections in CGD: two sides of a coin. Cell Mol Life Sci. Jan;69(1):7–15.
6. Ushio-Fukai M. Localizing NADPH oxidase-derived ROS. Sci STKE. 2006;2006(349):re8.
7. Matute JD, Arias AA, Wright NA, Wrobel I, Waterhouse CC, Li XJ, et al. A new genetic subgroup of chronic granulomatous disease with autosomal recessive mutations in p40 phox and selective defects in neutrophil NADPH oxidase activity. Blood. 2009;114(15):3309–15.
8. Park BH, Holmes BM, Rodey GE, Good RA. Nitroblue-tetrazolium test in children with fatal granulomatous disease and newborn infants. Lancet. 1969;1(7586):157.
9. Baehner RL, Nathan DG. Quantitative nitroblue tetrazolium test in chronic granulomatous disease. N Engl J Med. 1968;278(18):971–6.
10. Emmendorffer A, Hecht M, Lohmann-Matthes ML, Roesler J. A fast and easy method to determine the production of reactive oxygen intermediates by human and murine phagocytes using dihydrorhodamine 123. J Immunol Methods. 1990;131(2):269–75.
11. Roesler J, Hecht M, Freihorst J, Lohmann-Matthes ML, Emmendorffer A. Diagnosis of chronic granulomatous disease and of its mode of inheritance by dihydrorhodamine 123 and flow microcytofluorometry. Eur J Pediatr. 1991;150(3):161–5.
12. Salaria M, Singh S, Kumar L, Datta U, Sehgal S. Chronic granulomatous disease. Indian Pediatr. 1999;36(6):594–6.
13. Nair PS, Moorthy PK, Suprakasan S, Jayapalan S, Preethi K. Chronic granulomatous disease. Indian J Dermatol Venereol Leprol. 2005;71(3):199–201.
14. Pinto LM, Udwadia ZF. A 24-year-old man with giddiness, hemoptysis, and skin lesions. Chest. 2008;134(5):1084–7.
15. Soneja M, Batra A, Vikram NK, Ahuja A, Mohan A, Sood R. Actinomycosis and nocardiosis co-infection in chronic granulomatous disease. J Assoc Physicians India. Apr;60:66–8.
16. Verma S, Sharma PK, Sivanandan S, Rana N, Saini S, Lodha R, et al. Spectrum of primary immune deficiency at a tertiary care hospital. Indian J Pediatr. 2008;75(2):143–8.
17. Ahlin A, De Boer M, Roos D, Leusen J, Smith CI, Sundin U, et al. Prevalence, genetics and clinical presentation of chronic granulomatous disease in Sweden. Acta Paediatr. 1995;84(12):1386–94.
18. Liese J, Kloos S, Jendrossek V, Petropoulou T, Wintergerst U, Notheis G, et al. Long-term follow-up and outcome of 39 patients with chronic granulomatous disease. J Pediatr. 2000;137(5):687–93.
19. Koker MY, Camcioglu Y, van Leeuwen K, Kilic SS, Barlan I, Yilmaz M, et al. Clinical, functional, and genetic characterization of chronic granulomatous disease in 89 Turkish patients. J Allergy Clin Immunol. Jul 30.
20. El Kares R, Barbouche MR, Elloumi-Zghal H, Bejaoui M, Chemli J, Mellouli F, et al. Genetic and mutational heterogeneity of autosomal recessive chronic granulomatous disease in Tunisia. J Hum Genet. 2006;51(10):887–95.
21. Reich D, Thangaraj K, Patterson N, Price AL, Singh L. Reconstructing Indian population history. Nature. 2009;461(7263):489–94.
22. Martire B, Rondelli R, Soresina A, Pignata C, Broccoletti T, Finocchi A, et al. Clinical features, long-term follow-up and outcome of a large cohort of patients with Chronic Granulomatous Disease: an Italian multicenter study. Clin Immunol. 2008;126(2):155–64.
23. van den Berg JM, van Koppen E, Ahlin A, Belohradsky BH, Bernatowska E, Corbeel L, et al. Chronic granulomatous disease: the European experience. PLoS One. 2009;4(4):e5234.
24. Finn A, Hadzic N, Morgan G, Strobel S, Levinsky RJ. Prognosis of chronic granulomatous disease. Arch Dis Child. 1990;65(9):942–5.
25. van Montfrans JM, Rudd E, van de Corput L, Henter JI, Nikkels P, Wulffraat N, et al. Fatal hemophagocytic lymphohistiocytosis in X-linked chronic granulomatous disease associated with a perforin gene variant. Pediatr Blood Cancer. 2009;52(4):527–9.
26. Parekh C, Hofstra T, Church JA, Coates TD. Hemophagocytic lymphohistiocytosis in children with chronic granulomatous disease. Pediatr Blood Cancer. Mar;56(3):460–2.
27. Alvarez-Cardona A, Rodriguez-Lozano AL, Blancas-Galicia L, Rivas-Larrauri FE, Yamazaki-Nakashimada MA. Intravenous immunoglobulin treatment for macrophage activation syndrome complicating chronic granulomatous disease. J Clin Immunol. Apr;32(2):207–11.
28. Lee PP, Chan KW, Jiang L, Chen T, Li C, Lee TL, et al. Susceptibility to mycobacterial infections in children with X-linked chronic granulomatous disease: a review of 17 patients living in a region endemic for tuberculosis. Pediatr Infect Dis J. 2008;27(3):224–30.
29. Bustamante J, Aksu G, Vogt G, de Beaucoudrey L, Genel F, Chapgier A, et al. BCG-osis and tuberculosis in a child with chronic granulomatous disease. J Allergy Clin Immunol. 2007;120(1):32–8.
30. Bustamante J, Arias AA, Vogt G, Picard C, Galicia LB, Prando C, et al. Germline CYBB mutations that selectively affect macrophages in kindreds with X-linked predisposition to tuberculous mycobacterial disease. Nat Immunol. Mar;12(3):213–21.
31. Hasui M. Chronic granulomatous disease in Japan: incidence and natural history. The Study Group of Phagocyte Disorders of Japan. Pediatr Int. 1999;41(5):589–93.
32. Mouy R, Fischer A, Vilmer E, Seger R, Griscelli C. Incidence, severity, and prevention of infections in chronic granulomatous disease. J Pediatr. 1989;114(4 Pt 1):555–60.
33. Roos D, Kuhns DB, Maddalena A, Roesler J, Lopez JA, Ariga T, et al. Hematologically important mutations: X-linked chronic granulomatous disease (third update). Blood Cells Mol Dis. Oct 15;45(3):246–65.
34. Roos D, Kuhns DB, Maddalena A, Bustamante J, Kannengiesser C, de Boer M, et al. Hematologically important mutations: the autosomal recessive forms of chronic granulomatous disease (second update). Blood Cells Mol Dis. Apr 15;44(4):291–9.
35. Casimir CM, Bu-Ghanim HN, Rodaway AR, Bentley DL, Rowe P, Segal AW. Autosomal recessive chronic granulomatous disease caused by deletion at a dinucleotide repeat. Proc Natl Acad Sci U S A. 1991;88(7):2753–7.
36. Gorlach A, Lee PL, Roesler J, Hopkins PJ, Christensen B, Green ED, et al. A p47-phox pseudogene carries the most common mutation causing p47-phox- deficient chronic granulomatous disease. J Clin Invest. 1997;100(8):1907–18.
37. Kuhns DB, Alvord WG, Heller T, Feld JJ, Pike KM, Marciano BE, et al. Residual NADPH oxidase and survival in chronic granulomatous disease. N Engl J Med. Dec 30;363(27):2600–10.

Immunology
The Journal of cells, molecules, systems and technologies
British Society for immunology

IMMUNOLOGY ORIGINAL ARTICLE

CD8$^+$ CD122$^+$ regulatory T cells contain clonally expanded cells with identical CDR3 sequences of the T-cell receptor β-chain

Yusuke Okuno,[1,2] Ayako Murakoshi,[1,2] Masashi Negita,[2] Kazuyuki Akane,[1] Seiji Kojima[1] and Haruhiko Suzuki[2]

[1]*Department of Paediatrics, Nagoya University Graduate School of Medicine, Nagoya, and* [2]*Department of Immunology, Nagoya University Graduate School of Medicine, Nagoya, Japan*

doi:10.1111/imm.12067
Received 04 July 2012; revised 26 December 2012; accepted 07 January 2013.
Correspondence: Dr Haruhiko Suzuki, Department of Immunology, Nagoya University Graduate School of Medicine, 65 Tsurumai-cho, Showa-ku, Nagoya 466-8550, Japan. Email: harusuzu@med.nagoya-u.ac.jp
Senior author:Ken-ichi Isobe, email: kisobe@med.nagoya-u.ac.jp

Summary

We identified CD8$^+$ CD122$^+$ regulatory T cells (CD8$^+$ CD122$^+$ Treg cells) and reported their importance in maintaining immune homeostasis. The absence of CD8$^+$ CD122$^+$ Treg cells has been shown to lead to severe systemic autoimmunity in several mouse models, including inflammatory bowel diseases and experimental autoimmune encephalomyelitis. The T-cell receptors (TCRs) expressed on CD8$^+$ CD122$^+$ Treg cells recognize the target cells to be regulated. To aid in the identification of the target antigen(s) recognized by TCRs of CD8$^+$ CD122$^+$ Treg cells, we compared the TCR diversity of CD8$^+$ CD122$^+$ T cells with that of conventional, naive T cells in mice. We analysed the use of TCR-Vβ in the interleukin 10-producing population of CD8$^+$ CD122$^+$ T cells marked by high levels of CD49d expression, and found the significantly increased use of Vβ13 in these cells. Immunoscope analysis of the complementarity-determining region 3 (CDR3) of the TCR β-chain revealed remarkable skewing in a pair of Vβ regions, suggesting the existence of clonally expanded cells in CD8$^+$ CD122$^+$ T cells. Clonal expansion in Vβ13$^+$ cells was confirmed by determining the DNA sequences of the CDR3s. The characteristic TCR found in this study is an important building block for further studies to identify the target antigen recognized by CD8$^+$ CD122$^+$ Treg cells.

Keywords: CD8$^+$; diversity; regulatory T cells; T-cell receptor.

Introduction

Regulatory T (Treg) cells have been intensively studied in the field of immunology. They have been shown to be an important T-cell subset for maintaining immune homeostasis.[1,2] Of these, the most extensively studied Treg cells are CD4$^+$ CD25$^+$ Foxp3$^+$ Treg cells.[3] Their important function is shown by the phenotype of Foxp3-deficient mice, which have severe systemic autoimmune diseases.[4,5] Interleukin-10 (IL-10), transforming growth factor-β, cytotoxic T-lymphocyte antigen 4 and glucocorticoid-induced tumour necrosis factor-receptor are reported to be key effector molecules for CD4$^+$ CD25$^+$ Foxp3$^+$ Treg cells.[6] Clinical trials based on CD4$^+$ CD25$^+$ Foxp3$^+$ Treg cell studies are underway.[7] Other Treg cells, including type 1 (Tr1) cells, CD8$\alpha\alpha$ TCR-$\alpha\beta$ Treg cells and CD8$^+$ CD122$^+$ Treg cells have been reported.[8–10]

Our study group has identified CD8$^+$ CD122$^+$ Treg cells in mice and reported their role in multiple disease models, including experimental autoimmune encephalomyelitis and inflammatory bowel diseases.[11,12] Another group has identified their potential contribution to autoimmune thyroiditis.[13] In the absence of CD8$^+$ CD122$^+$ Treg cells, activation of autoreactive T cells in these models became aggressive, suggesting their importance in maintaining immune homeostasis. It was also proposed that CD8$^+$ CD122$^+$ Treg cells in association with CD4$^+$ CD25$^+$ Foxp3$^+$ Treg cells suppress autoreactive T cells.[12] Interleukin-10 is an important effector molecule for CD8$^+$ CD122$^+$ Treg cells to suppress the activation of conventional T cells *in vitro*.[14] We have also reported that human peripheral blood does not contain CD8$^+$ CD122$^+$ cells; however, the functional human counterpart of murine CD8$^+$ CD122$^+$ Treg cells can be marked with CD8$^+$ CXCR3$^+$ cells.[15]

Recently, Dai *et al.*[16] reported that programmed death 1 (PD-1) expression discriminates CD8$^+$ CD122$^+$ Treg cells from CD8$^+$ memory T cells. Because CD122 has historically been used as a marker for mouse CD8$^+$ memory

Abbreviations: FAM, 5-carboxyfluorescein; IL-10, interleukin-10; MLN, mesenteric lymph nodes; PD-1, programmed death-1; PE, phycoerythrin; TCR, T-cell receptor; Treg, regulatory T

T cells,[17] $CD8^+$ $CD122^+$ cells possibly consist of memory T cells and Treg cells, although the number of memory T cells seems to be higher than the number of Treg cells. In the above-mentioned study, the authors showed that $CD8^+$ $CD122^+$ $PD\text{-}1^+$ cells mainly produced IL-10 in the $CD8^+$ population *in vitro*, and that they possessed *in vivo* regulatory activity to suppress T cells activated by an MHC-mismatched skin graft. PD-1 marks $CD8^+$ Treg cells more specifically in combination with CD122 and may enable a much more detailed study of $CD8^+$ $CD122^+$ Treg cells.

Determining the target antigen of the T-cell receptor (TCR) in a T-cell population is of vital importance for directly understanding their function to a specific antigen.[18,19] Indeed, many studies identifying the target antigens of cytotoxic T lymphocytes have been reported.[20] In contrast, only a few studies identifying the target antigens of $CD4^+$ $CD25^+$ $Foxp3^+$ Treg cells have been reported. Nonetheless, information of the target antigen recognized by $CD4^+$ $CD25^+$ $Foxp3^+$ Treg cells has revealed that stimulation is important for their suppressive activity against naive T cells.[21,22]

Before identifying the target antigen recognized by $CD8^+$ $CD122^+$ Treg cells, we studied the TCR diversity of $CD8^+$ $CD122^+$ T cells. We followed a conventional approach for analysing the T-cell response to non-self antigens. Flow cytometric analysis with antibodies specific for each Vβ region, immunoscope analysis, and determination of the DNA sequence around complementarity-determining region 3 (CDR3) of the TCR-β gene revealed a skewed use of TCRs in $CD8^+$ $CD122^+$ T cells. This skewing of TCR diversity in $CD8^+$ $CD122^+$ T cells is possibly generated by the clonal expansion of Treg cells or memory T cells responding to the target T cells rather than by the skewed formation of TCRs during T-cell differentiation.

Materials and methods

Mice

C57BL/6J female mice (6–8 weeks old, unless specified) were purchased from Japan SLC (Hamamatsu, Japan). All mice used in this study were maintained in a specific pathogen-free environment. Animal care was performed according to the guidelines of Nagoya University (Nagoya, Japan). Experimental protocols were approved by the Ethics Committee of the Nagoya University Graduate School of Medicine (No. 22310 and 23024).

Flow cytometry

Phycoerythrin (PE)/indotricarbocyanine (Cy7)-conjugated anti-mouse CD8a (clone 53-6·7), biotin-conjugated anti-mouse CD122 (clone 5H4), PE-conjugated anti-mouse PD-1 (clone 29F.1A12), PE-conjugated anti-mouse TCR Vβ13 (clone MR12-4), and allophycocyanin-conjugated streptavidin were purchased from BioLegend (San Diego, CA). The PE-conjugated anti-mouse CD49d (clone 9C10) and mouse Vβ TCR Screening Panel (Cat. No 557004) were purchased from BD Biosciences (San Jose, CA). Cells (1×10^6) were stained with each antibody on ice for 20 min, and were then analysed using the FACSCantoII flow cytometer (BD Biosciences). For secondary staining of biotin-conjugated antibodies, cells were centrifuged at 600 ***g*** for 3 min, and the cell pellet was suspended in staining buffer with fluorochrome-conjugated streptavidin.

In vitro IL-10 production assay

Cell culture plates (96 wells per plate) were coated with 10 μg/ml anti-CD3 (clone 13C11; eBioscience, San Diego, CA) in PBS. Plates were washed with culture media; then, 1×10^5 cells were cultured in 200 µl RPMI-1640 medium (Sigma, St Louis, MO) supplemented with 50 U/ml penicillin, 50 μg/ml streptomycin (Invitrogen, Carlsbad, CA), 50 μM 2-mercaptoethanol (Invitrogen) and 10 ng/ml recombinant human IL-2 (Peprotech, Rocky Hill, NJ) for 48 hr. Culture supernatants were harvested, and the IL-10 concentration was measured using the mouse IL-10 Quantikine ELISA kit (R&D Systems, Minneapolis, MN) according to the manufacturer's instructions.

Reverse transcription-polymerase chain reaction

$CD8^+$ $CD122^-$, $CD8^+$ $CD122^+$ $CD49d^{low}$ and $CD8^+$ $CD122^+$ $CD49d^{high}$ cells from either the spleens or lymph nodes were sorted using the FACSAriaII cell sorter (BD Biosciences). For RNA extraction and immunoscope analysis, we collected 10^6 cells of all three populations. RNA was isolated using the RNeasy Micro Kit (Qiagen, Valencia, CA). The cDNA was synthesized with SuperScript III reverse transcriptase (Invitrogen) using random hexamer primers and was synthesized from the same amount of RNA of all three populations, suspended in the same amount (e.g. 20 µl) of double-distilled H_2O, and kept at – 20°.

Immunoscope analysis

Amplification of the CDR3 DNA region of each Vβ was performed by pairing each Vβ-specific primer with a Cβ-specific primer labelled with 5-carboxyfluorescein (FAM) at the 5′ end.[23] The sequence of each primer is listed in Table 1. For the further analysis of Vβ13–Jβ amplification, a Vβ13-specific primer was labelled with FAM and the sequence of each Jβ primer is listed in the Supplementary material, Table S1. For the analysis of Vα–Cα amplification, Cα-specific primer was labelled with FAM and the sequence of each Vα primer is listed in the Supplementary material, Table S2. First, 10^6 cells were prepared from each cell population ($CD8^+$ $CD122^-$, $CD8^+$ $CD122^+$ $CD49d^{low}$ and

Table 1. Primer sequences used for immunoscope analysis 1

Family	Sequences 5′–3′
Vβ1	CTGAATGCCCAGACAGCTCCAGC
Vβ2	TCACTGATACGGAGCTGAGGC
Vβ3	CCTTGCAGCCTAGAAATTCAGT
Vβ4	GCCTCAAGTCGCTTCCAACCTC
Vβ5.2	AAGGTGGAGAGAGACAAAGGATTC
Vβ6	CTCTCACTGTGACATCTGCCC
Vβ7	TACAGGGTCTCACGGAAGAAGC
Vβ8.2	CATTATTCATATGGTGCTGGC
Vβ8.3	TGCTGGCAACCTTCGAATAGGA
Vβ9	TCTCTCTACATTGGCTCTGCAGGC
Vβ10	ATCAAGTCTGTAGAGCCGGAGGA
Vβ11	GCACTCAACTCTTGAAGATCCAGAGC
Vβ12	GATGGTGGGGCTTTCAAGGATC
Vβ13	AGGCCTAAAGGAACTAACTCCCAC
Vβ14	ACGACCAATTCATCCTAAGCAC
Vβ15	CCCATCAGTCATCCCAACTTATCC
Vβ16	CACTCTGAAAATCCAACCCAC
Vβ18	CAGCCGGCCAAACCTAACATTCTC
Cβ-FAM	FAM-TTGGGTGGAGTCACATTTCTC

FAM: 5-carboxyfluorescein.

CD8$^+$ CD122$^+$ CD49d^{high}). Mice used to prepare the cells were identical for each cell population and the area of collecting cells in the cell sorter was finely adjusted so that the sorting time to obtain 10^6 cells should be approximately equal for each cell population. After cell sorting, cell number was counted and the same number (usually 10^6) of cells from three populations was used for the extraction of RNA. The cDNA was synthesized, suspended in the same amount (e.g. 20 μl) of double-distilled H_2O, and kept at −20°. The same amount of cDNA solution (e.g. 1 μl) was transferred into PCR mixture and the PCR was performed. PrimeSTAR GXL DNA polymerase (TaKaRa BIO Inc., Otsu, Japan) and the GeneAmp PCR System 2700 thermal cycler (Applied Biosystems, Foster City, CA) were used with the following temperature conditions: 98° for 10 seconds; 60° for 15 seconds; 68° for 20 seconds; for 30 cycles. The same amount of cDNA solution (e.g. 1 μl) was transferred into PCR mixture and the PCR was performed. Each PCR product was purified using capillary electrophoresis with an ABI 310 Genetic Analyzer (Applied Biosystems), according to the manufacturer's instructions. Results were analysed using the GeneMapper software (Applied Biosystems). In figures showing the results of the immunoscope analysis, the amplitude of each line was adjusted so that the highest peak in a single line reached near the top.

Sequencing analysis

The PCR was performed with PrimeSTAR GXL DNA polymerase. This reaction was performed using a Vβ-specific primer and a Cβ-specific primer. The PCR product was purified using Tris-saturated phenol : chloroform : isoamylalcohol (25 : 24 : 1), and an adenine-tail was added by *Ex Taq* DNA Polymerase (TaKaRa). The adenine-tailed PCR product was cloned using the pCR2.1-TOPO TA cloning kit (Invitrogen). Each CDR3 clone plasmid DNA was obtained, and the nucleotide sequence was analysed using the ABI BigDye 1.1 Cycle sequencing kit (Applied Biosystems) with the M13-reverse primer (5′-CAGGAAACAGCTATGAC-3′). The product was analysed with the ABI 310 Genetic Analyzer (Applied Biosystems). The resultant sequence data were analysed using Sequence Scanner software (Applied Biosystems) and IMGT/V-QUEST online software.[24]

Nomenclature

Gene names of Vβ, Jβ and Vα are according to the Immunogenetics (IMGT) gene name nomenclature for Immunoglobulin (Ig) and T cell Receptor (TR) of mice.[25–27]

Statistical analysis

Student's *t*-test with Bonferroni correction was used for each statistical analysis. *P*-values less than 0·05 divided by the number of comparisons were considered statistically significant.

Results

CD8$^+$ CD122$^+$ cells are separated into two subpopulations by CD49d expression

We have reported that CD122 could be used as a marker for CD8$^+$ Treg cells.[10] However, CD122 is also a classical marker for CD8$^+$ memory T cells[17]; therefore, CD8$^+$ CD122$^+$ cells could contain both memory and regulatory T cells. Dai *et al.*[16] reported that PD-1 expression defines subpopulations of CD8$^+$ CD122$^+$ cells. They showed that CD8$^+$ CD122$^+$ PD-1$^+$ cells mainly produced IL-10 *in vitro*, and that they suppressed rejection of allogeneic skin grafts *in vivo*. On the basis of these data, the authors concluded that PD-1$^+$ cells in the CD8$^+$ CD122$^+$ population are real regulatory cells. We found that CD49d (integrin-α4 chain) divides CD8$^+$ CD122$^+$ cells into two populations (CD122$^+$ CD49d^{low} cells and CD122$^+$ CD49d^{high} cells, Fig. 1a). Expression of CD49d in CD8$^+$ CD122$^+$ cells mostly correlated with that of PD-1 (Fig. 1b). CD8$^+$ CD122$^+$ CD49d^{high} cells, but not CD8$^+$ CD122$^+$ CD49d^{low} cells, produced IL-10 *in vitro* when stimulated with an anti-CD3 antibody (Fig. 1c). This CD8$^+$ CD122$^+$ CD49d^{high} cell subset was sustained until the mice were at least 20 weeks of age (Fig. 1d). On the basis of these results, subsequent experiments focused on CD8$^+$ CD122$^+$ CD49d^{high} cells rather than CD8$^+$ CD122$^+$ CD49d^{low} cells, and their TCR diversity was compared with that of CD8$^+$ CD122$^-$ cells (conventional, naive T cells).

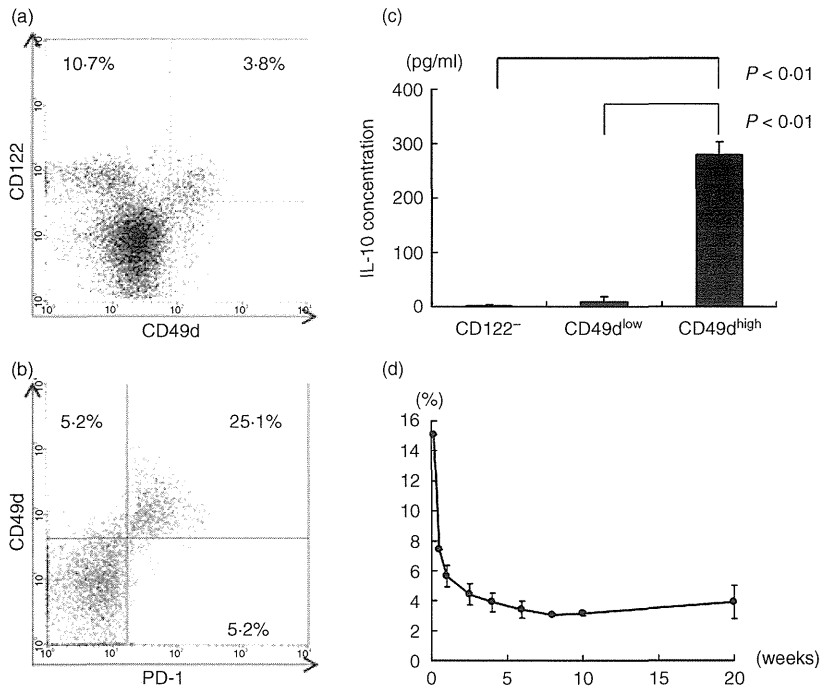

Figure 1. Characteristics of CD49d^{high} and CD49d^{low} cells in CD8$^+$ CD122$^+$ cells. (a) FACS analysis of spleen cells obtained from 6-week-old female C57BL/6 mice. Cells were stained with anti-CD8a, anti-CD122 and anti-CD49d antibodies. Expression pattern of CD49d and CD122 in CD8$^+$ cells is shown. A representative result among more than 10 experiments is presented. (b) Expression profile of programmed death 1 (PD-1) and CD49d in the CD8$^+$ CD122$^+$ population. Spleen cells were stained with anti-CD8a, anti-CD122, anti-CD49d and anti-PD-1 antibodies. Only CD8$^+$ CD122$^+$ cells are shown in the plot. (c) CD8$^+$ CD122$^-$, CD8$^+$ CD122$^+$ CD49d^{low} and CD8$^+$ CD122$^+$ CD49d^{high} cells were collected from spleen cells using a cell sorter and 10^5 cells per well were stimulated with plate-bound anti-CD3 antibody *in vitro* for 48 hr. Interleukin 10 (IL-10) concentration in the culture supernatant was measured by ELISA. Results are shown as mean ± standard deviation (SD). This result is representative of more than five independent experiments performed. (d) Percentage of CD8$^+$ CD122$^+$ CD49d^{high} cells in mice of various ages. Spleen cells obtained from mice of the indicated age were analysed. In each experiment, more than 10^5 cells obtained from a single mouse were analysed in a single experiment except when cells were collected from two to four mice in the case of neonates. Percentages of CD8$^+$ CD122$^+$ CD49d^{high} cells in CD8$^+$ populations are shown as mean ± SD. Results are obtained from at least three independent experiments.

CD8$^+$ CD122$^+$ CD49d^{high} cells had skewed Vβ usage in mesenteric lymph nodes

We compared TCR Vβ usage of CD8$^+$ CD122$^+$ C-D49d^{high} cells and CD8$^+$ CD122$^+$ CD49d^{low} cells with that of CD8$^+$ CD122$^-$ cells. Cells were stained with a panel of each Vβ-specific antibody, and the percentage of cells that used each Vβ was determined using flow cytometric analysis. In the spleens of wild-type mice, no statistically significant differences were observed in the percentage of each Vβ^+ cell in the three populations (Fig. 2a). However, in mesenteric lymph nodes (MLNs), the percentage of Vβ13$^+$ cells was significantly higher in CD8$^+$ CD122$^+$ CD49d^{high} cells (10%) than in CD8$^+$ C-D122$^-$ cells (4%, $P < 0{\cdot}01$) or CD8$^+$ CD122$^+$ CD49d^{low} cells (5%, $P < 0{\cdot}01$), suggesting an increase in CD8$^+$ CD122$^+$ CD49d^{high} Vβ13$^+$ cells in MLNs (Fig. 2b).

Immunoscope analysis of CDR3 regions of TCRs showed different patterns among CD8$^+$ CD122$^+$ CD49d^{high} cells, CD8$^+$ CD122$^+$ CD49d^{low} cells and CD8$^+$ CD122$^-$ cells

Next, we examined TCR diversity of the CD8$^+$ T-cell populations using immunoscope analysis (Figs. 3a,b). The results showed several skewed peaks that were not observed in CD8$^+$ CD122$^-$ cells, but that were apparent in CD8$^+$ CD122$^+$ CD49d^{high} cells. There were also several skewed peaks in CD8$^+$ CD122$^+$ CD49d^{low} cells. There was a skewed peak in CD8$^+$ CD122$^+$ CD49d^{high} cells harbouring Vβ13, which was expected to be present on the basis of the analysis of Vβ usage.

CD8$^+$ CD122$^+$ cells have clonal expansion according to CDR3 sequencing results

We focused on Vβ13 and analysed the nucleotide sequences containing the CDR3 of TCR-β. cDNAs obtained by reverse transcription-PCR (RT-PCR) of CDR3 combined with Vβ13 in CD8$^+$ CD122$^+$ CD49d^{high} cells, CD8$^+$ CD122$^+$ CD49d^{low} cells and CD8$^+$ CD122$^-$ cells were cloned and compared with one another. In the clones analysed to determine the nucleotide sequences in each cell population, the most common CDR3 sequences

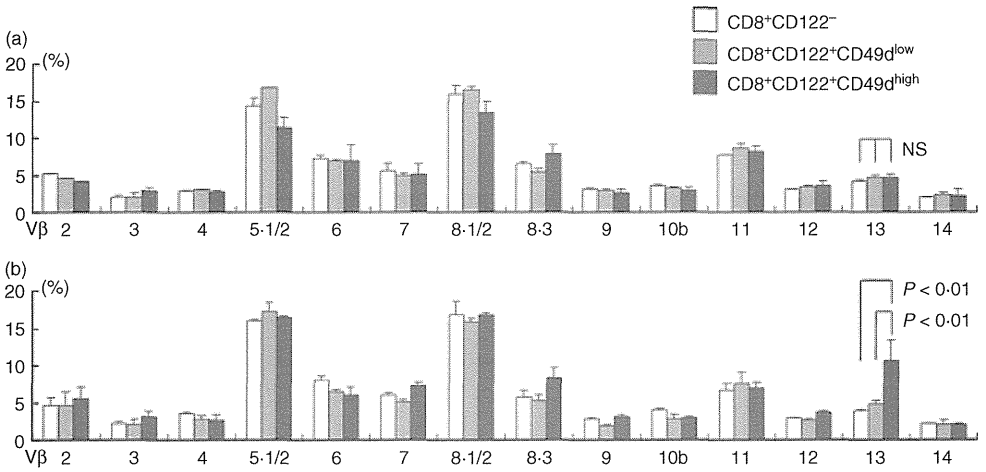

Figure 2. T-cell receptor (TCR) Vβ usage of CD8$^+$ T-cell subsets. (a) TCR Vβ usage of CD8$^+$ CD122$^-$ (white bars), CD8$^+$ CD122$^+$ CD49d^{low} (light grey bars) and CD8$^+$ CD122$^+$ CD49d^{high} cells (dark grey bars) in the spleen is shown. Spleen cells from 6-week-old C57BL/6 mice (1×10^6 cells for one staining) were stained with anti-CD8, anti-CD122, anti-CD49d, and each anti-Vβ-specific antibody; the percentages of each Vβ^+ cell in each cell subset are demonstrated as a graph. (b) Identical analysis of Vβ usage to (a) was performed except that the cells were obtained from mesenteric lymph nodes; 1×10^6 cells for one staining were also maintained for lymph node cells. Percentages of cells stained with each Vβ-specific antibody in each cell subset are shown as mean $\pm$ SD. Results were obtained from three independent experiments.

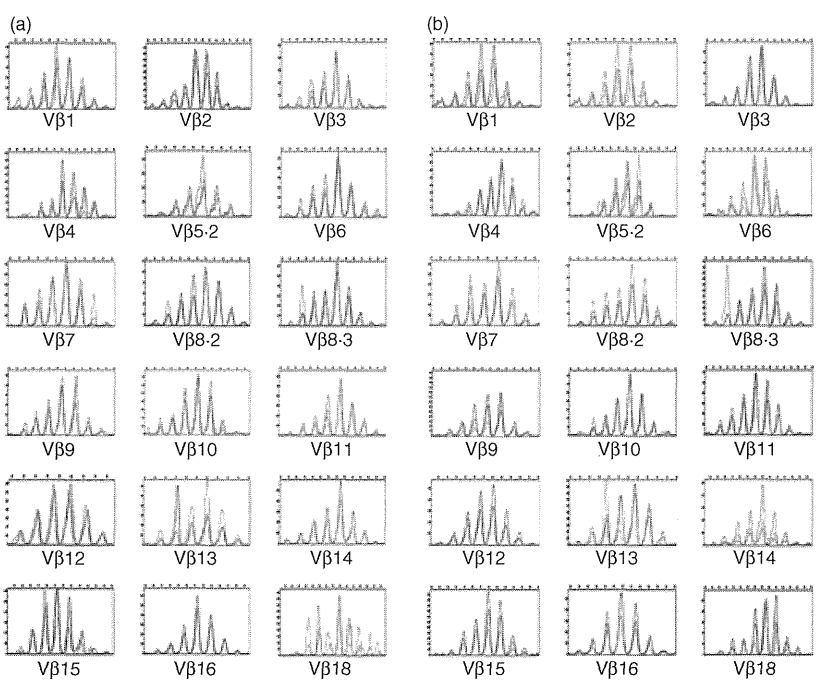

Figure 3. Immunoscope analysis. (a) Immunoscope analysis with Vβ-specific primers and Cβ primers was performed with cDNA obtained from CD8$^+$ CD122$^-$ (black lines), CD8$^+$ CD122$^+$ CD49d^{low} (blue lines) and CD8$^+$ CD122$^+$ CD49d^{high} (red lines) cells in (a) spleens and (b) mesenteric lymph nodes. Results are representative of two independent experiments.

are listed in Fig. 4. There was only one CDR3 sequence that appeared twice during DNA sequence analysis of CD8$^+$ CD122$^-$ cells (Fig. 4c). In comparison with the result obtained from CD8$^+$ CD122$^-$ cells, three different CDR3 sequences were found twice in CD8$^+$ CD122$^+$ CD49d^{low} cells (Fig. 4b), possibly suggesting a higher frequency of expanded clones in this cell population. In contrast with the reasonably divergent CDR3 sequences in CD8$^+$ CD122$^-$ cells, identical CDR3 sequences were frequently found in CD8$^+$ CD122$^+$CD49d^{high} cells. In particular, one CDR3 sequence (ASSYRGAEQF) was found five times in the first experiment and six times in the second independent experiment, which suggests the expansion of T cells possessing one characteristic TCR β-chain

(a)
$CD8^+CD122^+CD49^{high}$ cells (Exp. 1)

V β	J β	CDR3	Frequency
13	2·1	ASSYRGAEQF	5/61
13	2·3	ASSPRGASAETLY	2/61
13	1·4	ASSWTLSNERLF	2/61
13	2·3	ASSLGASAETLY	2/61
13	2·7	ASRPGTGGGEQY	2/61
13	2·7	ASSPGLGGEQY	2/61
13	1·1	ASSFRNTEVF	2/61

$CD8^+CD122^+CD49^{high}$ cells (Exp. 2)

V β	J β	CDR3	Frequency
13	2·1	ASSYRGAEQF	6/76
13	2·7	ASSPGLGGEQY	4/76
13	2·1	ASSFNNYAEQF	3/76
13	2·3	ASSLGASAETLY	3/76
13	1·1	ASSFRNTEVF	2/76
13	2·7	ASSLGAGNTLY	2/76
13	2·1	ASSSTVYAEQF	2/76

(b)
$CD8^+CD122^+CD49d^{low}$ cells (Exp. 1)

V β	J β	CDR3	Frequency
13	2·7	ASSPGGYEQY	2/56
13	2·1	ASSFPGDNYAEQF	2/56
13	2·4	ASSLDRGSQNTLY	2/56

(c)
$CD8^+CD122^-$ cells (Exp. 1)

V β	J β	CDR3	Frequency
13	2·4	ASSFAGGENTLY	2/38

Figure 4. Complementarity-determining region 3 (CDR3)-sequence analysis. CDR3 DNA sequences of (a) $CD8^+$ $CD122^+$ $CD49d^{high}$ cells, (b) $CD8^+$ $CD122^+$ $CD49d^{low}$ cells and (c) $CD8^+$ $CD122^-$ cells were analysed by PCR using a Vβ13-specific primer and Cβ primer followed by determination of DNA sequences around CDR3. Amino acid sequences that appeared more than twice are shown with the number of clones with identical sequences in the total number of clones sequenced. Results were obtained from two independent experiments.

(Fig. 4a). Exp. 1 and Exp. 2 in Figure 4 were totally independent experiments started from different mice, from which we obtained four common sequences. This result confirms that such cloning of identical TCRs from different mice is the reflection of universal events occurring in every mouse, not the accidental events that occurred in some cloning step. These CDR3 sequence data are consistent with the data from the immunoscope analysis. The most frequent sequence observed in $CD8^+$ $CD122^+$ $CD49d^{high}$ cells (ASSYRGAEQF) and possibly by addition of sequences with the same length (e.g. ASSFRNTEVF) corresponded to the highest peak in the immunoscope analysis of Vβ13 left side peak of the red line in Fig. 3a), which was not observed in $CD8^+$ $CD122^+$ $CD49d^{low}$ cells and $CD8^+$ $CD122^-$ cells.

Further immunoscope analysis

We further analysed cDNA obtained from $CD8^+$ $CD122^-$ cells, $CD8^+$ $CD122^+$ $CD49d^{high}$ cells, $CD8^+$ $CD122^+$ $CD49d^{low}$ cells by immunoscope using primers for TCR Jβ combined with Vβ13, and some Vαs combined with Cα. The results of Vβ13-Jβ and Vα-Cα are shown in the Supplementary material, Fig. S1a and S1b, respectively. Although, the immunoscopic analysis using Jβ primers showed some skewed peaks as expected, it gave no further information than the analysis by Vβs-Cβ There was no clonal or oligoclonal enrichment of specific amplification of TCR clones, which would attract our attention to go into further analysis. By the analysis of α-chain by immunoscope of 11 different Vαs, we have not found any remarkable skewing of peaks in $CD8^+$ $CD122^+$ $CD49d^{high}$ cells or $CD8^+$ $CD122^+$ $CD49d^{low}$ cells. We only analysed 11 different Vαs to represent all the Vαs, which are estimated to be around 100. Judged from the result of immunoscope assays using 11 primers corresponding to the 11 different Vα segments, we did not perform further immunoscopic analysis using other Vα primers.

Immunoscope analysis of very young mice

To assess whether clonal expansion occurred as a result of the advantage in thymic selection or superior proliferative capacity in the periphery, we analysed the spectratype of T cells obtained from neonatal mice. $CD8^+$ $CD122^+$ $CD49d^{high}$ cells obtained from day-4 spleens had no detectable skewing of TCR length diversity in immunoscope analysis compared with those obtained from spleens of 6-week-old mice, indicating that clonal expansion causing skewing of TCR diversity occurred in mature T cells as the result of proliferation in the periphery (Fig. 5).

Discussion

We studied TCR diversity of $CD8^+$ $CD122^+$ cells using CD49d. Expression of CD49d in $CD8^+$ $CD122^+$ cells seemed to correlate with that of PD-1 (Fig. 1b); PD-1 expression has been shown to indicate Treg cells.[16] Although we have not investigated the regulatory function of $CD8^+$ $CD122^+$ $CD49d^{high}$ cells, such a correlation between PD-1 and CD49d suggests that $CD8^+$ $CD122^+$ $CD49d^{high}$ cells also contain functional Treg cells similar to $CD8^+$ $CD122^+$ $PD\text{-}1^+$ cells. We also observed that the proportion of $CD122^+$ $CD49d^{high}$ cells among total $CD8^+$

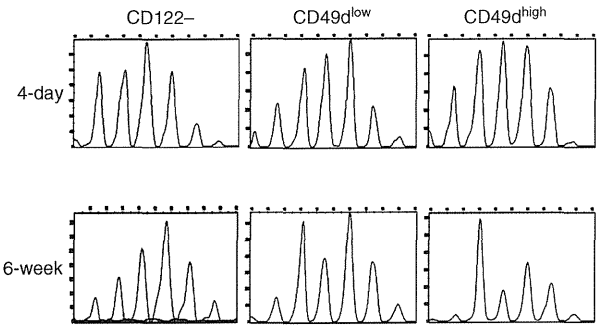

Figure 5. Immunoscope analysis of neonatal T cells. The cDNA of cell subsets sorted from the spleens of 4-day-old and 6-week-old mice were analysed with the Vβ13-specific primer in combination with the Cβ primer. Results are representative of two independent experiments.

T cells was high (~ 15%) in neonates or very young mice. Although we cannot address the meaning and mechanism of this phenomenon at present, it strongly correlates with our previous observation of a high proportion of CD122$^+$ cells among total CD8$^+$ T cells.[10] It is known that the CD8$^+$ CD122$^+$ population contains memory T cells[16] and such CD8$^+$ CD122$^+$ T cells appear in very young mice.[28] Although these CD8$^+$ CD122$^+$ T cells were thought to be memory T cells because they quickly responded to stimulations and produced interferon-γ, it may also be possible to designate these CD8$^+$ CD122$^+$ cells as regulatory cells. In fact, we observed that CD8$^+$ CD122$^+$ CD49d^{high} cells produced both IL-10 and interferon-γ when the cells were stimulated by anti-CD3 and anti-CD28 antibody-coated beads (our unpublished observation). If such CD8$^+$ CD122$^+$ memory T cells develop early and appear in very young mice, CD8$^+$ CD122$^+$ Treg cells may also develop earlier than conventional CD8$^+$ CD122$^-$ T cells to avoid a condition without Treg cells because conventional CD8$^+$ CD122$^-$ T cells, once activated by responding to either self or non-self antigens, may stay in the activated state and produce harmful levels of cytokines without regulation by CD8$^+$ Treg cells.[10]

In the initial flow cytometric analysis using a panel of anti-Vβ-specific antibodies, skewed use of Vβ13 was found in CD8$^+$ CD122$^+$ CD49d^{high} cells obtained from MLNs (Fig. 2b). This skewed use of Vβ13 was not observed in the cells obtained from spleens (Fig. 2a), suggesting a different distribution of CD8$^+$ Treg cells among lymphatic organs. The rationale for this skewed use of Vβ13 may be of future interest. There may be an unknown function of CD8$^+$ CD122$^+$ Treg cells in the intestine. The data presented here may correlate with data in our previous study, which showed that CD8$^+$ CD122$^+$ Treg cells inhibit colitogenic CD4$^+$ CD45RB^{high} cells *in vivo*.[12] However, immunoscope analysis showed a similar pattern between CD8$^+$ CD122$^+$ CD49d^{high} cells obtained from MLNs (Fig. 3a) and spleens (Fig. 3b), which suggests that the results from flow cytometric analysis were the result of the lower sensitivity of this technique compared with immunoscope analysis.

CD8$^+$ CD122$^+$ CD49d^{high} cells display a different use of their TCR from other CD8$^+$ T-cell populations. Such limited diversity is probably generated by clonal expansion of mature CD8$^+$ CD122$^+$ CD49d^{high} cells in the periphery rather than by preferential formation of TCR diversity in the thymus because such skewing of TCR diversity is not observed in the same CD8$^+$ CD122$^+$CD49d^{high} cell population obtained from neonatal (4-day-old) mice. We investigated whether CD8$^+$ CD122$^+$CD49d^{high} cells carrying the characteristic TCR are preferentially selected in the thymus or expanded in the periphery. The data obtained from analysing neonate spleen T cells suggest that they expanded in the periphery during the course of immune constitution (Fig. 5). In neonates, lymphopenia-induced homeostatic proliferation occurs, which leads to generation of T cells with an activated phenotype,[29] CD8$^+$ CD122$^+$ Treg cells may recognize these activated T cells and expand during this period.

Understanding TCR diversity is of considerable importance. Several studies have examined TCR diversity of CD4$^+$ CD25$^+$ Foxp3$^+$ Treg cells.[30,31] In neutral conditions, the TCR of CD4$^+$ CD25$^+$ Foxp3$^+$ Treg cells is diverse.[32,33] We found characteristically skewed TCR use in CD8$^+$ CD122$^+$ CD49d^{high} cells, which is different from that in CD4$^+$ CD25$^+$ Foxp3$^+$ Treg cells. Although we have not identified the mechanism underlying such skewed TCR use in CD8$^+$ CD122$^+$ CD49d^{high} cells, and possibly in CD8$^+$ CD122$^+$ CD49d^{low} cells as well, one possibility is that CD8$^+$ CD122$^+$ CD49d^{high} cells and/or CD8$^+$ CD122$^+$ CD49d^{low} cells may be constantly making contact with activated T cells that are also constantly generated because of exposure to exogenous antigens. In a previous study, we proposed that CD8$^+$ CD122$^+$ Treg cells recognize antigens selectively expressed in activated T cells to exceed regulatory activity.[34] On the basis of this hypothesis, we may be able to identify the target antigen recognized by CD8$^+$ CD122$^+$ Treg cells with the traditional method used for cytotoxic T lymphocytes, i.e. expression cloning from a cDNA library prepared from target cells. To study the characteristic TCR of CD8$^+$ CD122$^+$ Treg cells, namely that of Vβ13$^+$ cells, will lead to the identification of their target antigen, which may provide insight into understanding their function.

By comparing the immunoscopic profile between CD8$^+$ CD122$^+$ CD49d$^+$ cells and CD8$^+$ CD122$^-$ cells using Vβ13 and Jβ primers, there are some skewing peaks in CD8$^+$ CD122$^+$ CD49d$^+$ cells but they do not appear to be clonal or oligoclonal. It looks not much different from the analysis by various Vβ-Cβ immunoscopic analyses. From the sequence-determining analysis of Vβ13$^+$ cells, the TCR clonality was less than 10% in the most fre-

quently appeared clone, suggesting difficulty in showing clonality in the immunoscopic analysis by this case. The sequencing analysis showed the most frequently appeared clone to be Jβ2.1 and the immunoscope analysis of Vβ13-Jβ2.1 showed a skewed peak in $CD8^+$ $CD122^+$ $CD49d^{high}$ cells but the overall shape was not much different from that of Vβ13-Cβ.

A limitation of this study is that we did not show a relationship between each TCR and the regulatory function of the cells; this could be investigated by establishing many $CD8^+$ $CD122^+$ Treg cell clones, and then determining the regulatory function of the clones that possess the preferential CDR3 sequences detected in this study. Unfortunately, we have not succeeded in establishing functional $CD8^+$ $CD122^+$ Treg cell clones yet because these Treg cells lose their proliferating capacity in *in vitro* culture (our unpublished observation). It is difficult to determine the function of clonally expanded Treg cells obtained from wild-type mice because of the lack of methodology to purify a population with a single type of TCR. It may be necessary to make a number of lines of TCR transgenic mice to determine the function of T cells carrying one specific TCR.

The interpretation of this study is limited by the lack of a conclusion as to which subset of $CD8^+$ $CD122^+$ $CD49d^{high}$ or $CD8^+$ $CD122^+$ $CD49d^{low}$ cells are Treg cells. The study of PD-1^+ cells in the $CD8^+$ $CD122^+$ population by Dai *et al.*[16] and correlation of expression between PD-1 and CD49d (Fig. 1b) strongly suggests $CD8^+$ $CD122^+$ $CD49d^{high}$ cells as Treg cells, while the possibility of $CD49d^{low}$ as Treg cells still remains unknown (our unpublished observation). It has been demonstrated that memory T cells have skewed TCR diversity,[35] whereas there is little information regarding the TCR diversity of $CD8^+$ Treg cells. In this study, we observed an increased number of identical clones of TCR Vβ CDR3 (Fig. 4) in both $CD8^+$ $CD122^+$ $CD49d^{high}$ and $CD8^+$ $CD122^+$ $CD49d^{low}$ populations compared with that of the $CD8^+$ $CD122^-$ naive T-cell population, indicating clonal expansion of these CD122-expressing T cells. Importantly, identical clones were not shared between those obtained from the $CD49d^{high}$ population and the $CD49d^{low}$ population (Figs. 4a,b). This result indicates that two fundamentally different cell populations (probably Treg cells and memory T cells) are efficiently separated into the $CD8^+$ $CD122^+$ $CD49d^{low}$ population and the $CD8^+$ $CD122^+$ $CD49d^{high}$ population. Therefore, regardless of whether Treg cells are in the $CD8^+$ $CD122^+$ $CD49d^{low}$ population or in the $CD8^+$ $CD122^+$ $CD49d^{high}$ population, the conclusion that $CD8^+$ $CD122^+$ Treg cells have skewed TCR diversity is unchanged.

Acknowledgements

We thank Prof. Ken-ichi Isobe for financial help and useful discussions.

This work was supported by a Grant-in-Aid from the Japanese Ministry of Education, Culture, Science, Sports, and Technology, the Japanese Society for the Promotion of Science [grant number 20-08460], DAIKO Foundation, the 24th General Assembly of the Japanese Association of Medical Sciences, and The Waksman Foundation of Japan Inc.

Disclosures

The authors declare no financial or commercial conflict of interest.

References

1 Paust S, Cantor H. Regulatory T cells and autoimmune disease. *Immunol Rev* 2005; **204**:195–207.
2 Tang XL, Smith TR, Kumar V. Specific control of immunity by regulatory CD8 T cells. *Cell Mol Immunol* 2005; **2**:11–9.
3 Shevach EM, DiPaolo RA, Andersson J, Zhao DM, Stephens GL, Thornton AM. The lifestyle of naturally occurring $CD4^+$ $CD25^+$ $Foxp3^+$ regulatory T cells. *Immunol Rev* 2006; **212**:60–73.
4 Fontenot JD, Gavin MA, Rudensky AY. Foxp3 programs the development and function of $CD4^+$ $CD25^+$ regulatory T cells. *Nat Immunol* 2003; **4**:330–6.
5 Khattri R, Cox T, Yasayko SA, Ramsdell F. An essential role for Scurfin in $CD4^+$ $CD25^+$ T regulatory cells. *Nat Immunol* 2003; **4**:337–42.
6 Yong Z, Chang L, Mei YX, Yi L. Role and mechanisms of $CD4^+$ $CD25^+$ regulatory T cells in the induction and maintenance of transplantation tolerance. *Transpl Immunol* 2007; **17**:120–9.
7 Thumar JR, Kluger HM. Ipilimumab: a promising immunotherapy for melanoma. *Oncology (Williston Park)* 2010; **24**:1280–8.
8 Kim HJ, Verbinnen B, Tang X, Lu L, Cantor H. Inhibition of follicular T-helper cells by $CD8^+$ regulatory T cells is essential for self tolerance. *Nature* 2010; **467**:328–32.
9 Apetoh L, Quintana FJ, Pot C *et al.* The aryl hydrocarbon receptor interacts with c-Maf to promote the differentiation of type 1 regulatory T cells induced by IL-27. *Nat Immunol* 2010; **11**:854–61.
10 Rifa'i M, Kawamoto Y, Nakashima I, Suzuki H. Essential roles of $CD8^+$ $CD122^+$ regulatory T cells in the maintenance of T cell homeostasis. *J Exp Med* 2004;**200**: 1123–34.
11 Lee YH, Ishida Y. Rifa'i M, Shi Z, Isobe K, Suzuki H. Essential role of $CD8^+$ $CD122^+$ regulatory T cells in the recovery from experimental autoimmune encephalomyelitis. *J Immunol* 2008; **180**:825–32.
12 Endharti AT, Okuno Y, Shi Z, Misawa N, Toyokuni S, Ito M, Isobe K, Suzuki H. $CD8^+$ $CD122^+$ regulatory T cells (Tregs) and $CD4^+$ Tregs cooperatively prevent and cure $CD4^+$ cell-induced colitis. *J Immunol* 2011; **186**:41–52.
13 Saitoh O, Abiru N, Nakahara M, Nagayama Y. $CD8^+$ $CD122^+$ T cells, a newly identified regulatory T subset, negatively regulate Graves' hyperthyroidism in a murine model. *Endocrinology* 2007; **148**:6040–6.
14 Endharti AT, Rifa IM, Shi Z *et al.* Cutting edge: $CD8^+$ $CD122^+$ regulatory T cells produce IL-10 to suppress IFN-γ production and proliferation of $CD8^+$ T cells. *J Immunol* 2005; **175**:7093–7.
15 Shi Z, Okuno YRifa'i M, Endharti AT, Akane K, Isobe K, Suzuki H. Human $CD8^+$ $CXCR3^+$ T cells have the same function as murine $CD8^+$ $CD122^+$ Treg. *Eur J Immunol* 2009; **39**:2106–19.
16 Suzuki H, Shi Z, Okuno Y, Isobe K. Are $CD8^+$ $CD122^+$ cells regulatory T cells or memory T cells? *Hum Immunol* 2008; **69**:751–4.
17 Dai H, Wan N, Zhang S, Moore Y, Wan F, Dai Z. Cutting edge: programmed death-1 defines $CD8^+$ $CD122^+$ T cells as regulatory versus memory T cells. *J Immunol* 2010; **185**:803–7.
18 Sprent J, Surh CD. T cell memory. *Annu Rev Immunol* 2002; **20**:551–79.
19 Turner SJ, La Gruta NL, Kedzierska K, Thomas PG, Doherty PC. Functional implications of T cell receptor diversity. *Curr Opin Immunol* 2009; **21**:286–90.
20 Kedzierska K, La Gruta NL, Stambas J, Turner SJ, Doherty PC. Tracking phenotypically and functionally distinct T cell subsets via T cell repertoire diversity. *Mol Immunol* 2008; **45**:607–18.
21 Knuth A, Jager D, Jager E. Cancer immunotherapy in clinical oncology. *Cancer Chemother Pharmacol* 2000; **46**(Suppl):S46–51.
22 Nishikawa H, Kato T, Tawara I *et al.* Definition of target antigens for naturally occurring $CD4^+$ $CD25^+$ regulatory T cells. *J Exp Med* 2005; **201**:681–6.

23 Wang HY, Lee DA, Peng G, Guo Z, Li Y, Kiniwa Y, Shevach EM, Wang RF. Tumor-specific human CD4$^+$ regulatory T cells and their ligands: implications for immunotherapy. *Immunity* 2004; **20**:107–18.
24 Currier JR, Robinson MA. Spectratype/immunoscope analysis of the expressed TCR repertoire. *Current Protocols in Immunology* 2001; **38**:10.28.1–10.28.24.
25 Brochet X, Lefranc MP, Giudicelli V. IMGT/V-QUEST: the highly customized and integrated system for IG and TR standardized V-J and V-D-J sequence analysis. *Nucleic Acids Res* 2008;**36**(Web Server issue):W503–8.
26 Bosc N, Lefranc MP. The mouse (*Mus musculus*) T cell receptor α (TRA) and δ (TRD) variable genes. *Dev Comp Immunol* 2003; **27**:465–97.
27 Arden B, Clark SP, Kabelitz D, Mak TW. Mouse T-cell receptor variable gene segment families. *Immunogenetics* 1995; **42**:501–30.
28 Wilson RK, Lai E, Concannon P, Barth RK, Hood LE. Structure, organization and polymorphism of murine and human T-cell receptor α and β chain gene families. *Immunol Rev* 1988; **101**:149–72.
29 Ichii H, Sakamoto A, Hatano M *et al.* Role for Bcl-6 in the generation and maintenance of memory CD8$^+$ T cells. *Nat Immunol* 2002; **3**:558–63.
30 Schuler T, Hammerling GJ, Arnold B. Cutting edge: IL-7-dependent homeostatic proliferation of CD8$^+$ T cells in neonatal mice allows the generation of long-lived natural memory T cells. *J Immunol* 2004; **172**:15–9.
31 Daniely D, Kern J, Cebula A, Ignatowicz L. Diversity of TCRs on natural Foxp3$^+$ T cells in mice lacking Aire expression. *J Immunol* 2010; **184**:6865–73.
32 Pacholczyk R, Ignatowicz H, Kraj P, Ignatowicz L. Origin and T cell receptor diversity of Foxp3$^+$ CD4$^+$ CD25$^+$ T cells. *Immunity* 2006; **25**:249–59.
33 Fujishima M, Hirokawa M, Fujishima N, Sawada K. TCR$\alpha\beta$ repertoire diversity of human naturally occurring CD4$^+$ CD25$^+$ regulatory T cells. *Immunol Lett* 2005; **99**: 193–7.
34 Kasow KA, Chen X, Knowles J, Wichlan D, Handgretinger R, Riberdy JM. Human CD4$^+$ CD25$^+$ regulatory T cells share equally complex and comparable repertoires with CD4$^+$ CD25$^-$ counterparts. *J Immunol* 2004; **172**:6123–8.
35 Rifa'i M, Shi Z, Zhang SY, Lee YH, Shiku H, Isobe K, Suzuki H. CD8$^+$ CD122$^+$ regulatory T cells recognize activated T cells via conventional MHC class I-$\alpha\beta$TCR interaction and become IL-10-producing active regulatory cells. *Int Immunol* 2008;**20**:937–47.
36 Kurachi M, Kakimi K, Ueha S, Matsushima K. Maintenance of memory CD8$^+$ T cell diversity and proliferative potential by a primary response upon re-challenge. *Int Immunol* 2007; **19**:105–15.

Supporting Information

Additional Supporting Information may be found in the online version of this article:

Figure S1. (a) Immunoscope analysis with Vβ13-specific primers and Jβ primers was performed with cDNA obtained from CD8$^+$ CD122$^-$ (black lines), CD8$^+$ CD122$^+$ CD49d^{low} (blue lines) and CD8$^+$ CD122$^+$ CD49d^{high} (red lines) cells in mesenteric lymph nodes. (b) Immunoscope analysis with Vα-specific primers and Cα primers was performed with cDNA obtained from CD8$^+$ CD122$^-$ (black lines), CD8$^+$ CD122$^+$ CD49d^{low} (blue lines) and CD8$^+$ CD122$^+$ CD49d^{high} (red lines) cells in mesenteric lymph nodes.

Table S1. Primer sequences used for immunoscope analysis.

Table S2. Primer sequences used for immunoscope analysis.

nature genetics

Exome sequencing identifies secondary mutations of *SETBP1* and *JAK3* in juvenile myelomonocytic leukemia

Hirotoshi Sakaguchi[1,8], Yusuke Okuno[2,8], Hideki Muramatsu[1,8], Kenichi Yoshida[2,8], Yuichi Shiraishi[3], Mariko Takahashi[2], Ayana Kon[2], Masashi Sanada[2,4], Kenichi Chiba[3], Hiroko Tanaka[5], Hideki Makishima[6], Xinan Wang[1], Yinyan Xu[1], Sayoko Doisaki[1], Asahito Hama[1], Koji Nakanishi[1], Yoshiyuki Takahashi[1], Nao Yoshida[7], Jaroslaw P Maciejewski[6], Satoru Miyano[3,5], Seishi Ogawa[2,4,9] & Seiji Kojima[1,9]

Juvenile myelomonocytic leukemia (JMML) is an intractable pediatric leukemia with poor prognosis[1] whose molecular pathogenesis is poorly understood, except for somatic or germline mutations of RAS pathway genes, including *PTPN11*, *NF1*, *NRAS*, *KRAS* and *CBL*, in the majority of cases[2–4]. To obtain a complete registry of gene mutations in JMML, whole-exome sequencing was performed for paired tumor-normal DNA from 13 individuals with JMML (cases), which was followed by deep sequencing of 8 target genes in 92 tumor samples. JMML was characterized by a paucity of gene mutations (0.85 non-silent mutations per sample) with somatic or germline RAS pathway involvement in 82 cases (89%). The *SETBP1* and *JAK3* genes were among common targets for secondary mutations. Mutations in the latter were often subclonal and may be involved in the progression rather than the initiation of leukemia, and these mutations associated with poor clinical outcome. Our findings provide new insights into the pathogenesis and progression of JMML.

JMML is a rare myelodysplastic/myeloproliferative neoplasm unique to childhood, characterized by excessive proliferation of myelomonocytic cells and hypersensitivity to granulocyte-macrophage colony-stimulating factor[1]. A cardinal genetic feature of JMML is frequent somatic and/or germline mutation of RAS pathway genes, such as *NF1*, *NRAS*, *KRAS*, *PTPN11* and *CBL*, which are mutated in more than 70% of JMML cases in a mutually exclusive manner[2–4]. However, it is still open to question whether RAS pathway mutations are sufficient for the development of JMML or if secondary mutations have a role in the development and progression of this cancer. To address these issues and to better define the molecular pathogenesis of JMML, we performed whole-exome sequencing of paired tumor-normal DNA from 13 cases (**Supplementary Table 1**). We obtained mean coverage in exome sequencing of 137× for tumor samples and 143× for normal samples (**Supplementary Fig. 1**). A Monte-Carlo simulation indicated that the study detected 88% of the existing somatic mutations (Online Methods and **Supplementary Fig. 2**).

Sanger sequencing of 25 candidate non-silent somatic nucleotide alterations confirmed 1 nonsense and 10 missense mutations (**Table 1** and **Supplementary Fig. 3**), with the low true positive rate consistent with the very low numbers of somatic mutations in JMML. Of the 11 somatic mutations, 6 involved known RAS pathway genes. In addition, non-overlapping RAS pathway mutations (6 somatic and 6 germline) were confirmed in 11 of the 13 discovery cases (86%; **Table 1**). For the remaining two cases that lacked documented RAS pathway mutations, we intensively searched for possible germline mutations that could be relevant to the development of JMML. In total, 179 and 167 candidate germline mutations were detected in subjects 77 and 92, respectively, but these mutations did not affect known RAS pathway genes or other cancer-related genes, including the ones registered in the pathway databases (Online Methods). A frameshift deletion in *KMT2D* (also known as *MLL2*; encoding p.Val1670fs) was found in subject 92, who had been diagnosed as having Noonan syndrome on the basis of typical features such as hypertelorism, webbed neck and congenital heart disease (**Supplementary Fig. 3**) but lacked the distinctive facial appearance of Kabuki syndrome, which was shown to be caused by germline *KMT2D* mutations[5].

Five of the 11 somatic mutations were non–RAS pathway mutations, involving *SETBP1* (3 p.Asp868Asn alterations), *JAK3* (1 p.Arg657Gln alteration) and *SH3BP1* (1 p.Ser277Leu alteration), which had not been reported in JMML cases. SETBP1 was originally isolated as a 170-kDa nuclear protein that interacts with SET, a small protein inhibitor of the putative tumor suppressors PP2A and NM23-H1 (ref. 6). Several lines of recent evidence suggest that SETBP1 has a role in leukemogenesis (**Supplementary Fig. 4**)[7–11]. *SETBP1* participates in

[1]Department of Pediatrics, Nagoya University Graduate School of Medicine, Nagoya, Japan. [2]Cancer Genomics Project, Graduate School of Medicine, The University of Tokyo, Tokyo, Japan. [3]Laboratory of DNA Information Analysis, Human Genome Center, Institute of Medical Science, The University of Tokyo, Tokyo, Japan. [4]Department of Pathology and Tumor Biology, Graduate School of Medicine, Kyoto University, Kyoto, Japan. [5]Laboratory of Sequence Analysis, Human Genome Center, Institute of Medical Science, The University of Tokyo, Tokyo, Japan. [6]Department of Translational Hematology and Oncology Research, Taussig Cancer Institute, Cleveland Clinic, Cleveland, Ohio, USA. [7]Department of Hematology and Oncology, Children's Medical Center, Japanese Red Cross Nagoya First Hospital, Nagoya, Japan. [8]These authors contributed equally to this work. [9]These authors jointly directed this work. Correspondence should be addressed to S.O. (sogawa-tky@umin.ac.jp) or S.K. (kojimas@med.nagoya-u.ac.jp).

Received 6 November 2012; accepted 17 June 2013; published online 7 July 2013; doi:10.1038/ng.2698

Table 1 List of gene mutations identified by whole-exome sequencing

	RAS pathway mutations								Other somatic mutations			
	Somatic				Germline							
Subject number	Gene	Change at DNA level	Change at protein level	VAF[a]	Gene	Change at DNA level	Change at protein level	VAF[a]	Gene	Change at DNA level	Change at protein level	VAF[a]
11[b]	*NF1*	c.4537C>T	p.Arg1513*	40.1/24.2	*NF1*	c.5927delG	p.Trp1976fs	44.0/47.1	*SETBP1*	c.2602G>A	p.Asp868Asn	32.6/27.0
63	*KRAS*	c.38G>A	p.Gly13Asp	44.3/0.0	–	–	–	–	–	–	–	–
72	*PTPN11*	c.172A>T	p.Asn58Tyr	48.2/5.7	–	–	–	–	*SETBP1*	c.2602G>A	p.Asp868Asn	45.9/2.5
									JAK3	c.1970G>A	p.Arg657Gln	30.5/2.2
									SH3BP1	c.830C>T	p.Ser277Leu	47.8/5.1
77	–	–	–	–	–	–	–	–	*SETBP1*	c.2602G>A	p.Asp868Asn	33.4/2.1
78	*NRAS*	c.35G>C	p.Gly12Ala	45.5/9.5	–	–	–	–	–	–	–	–
82	–	–	–	–	*CBL*	c.1217del22	p.Thr406fs	34.7/38.9	–	–	–	–
83	–	–	–	–	*NF1*	c.4970A>G	p.Tyr1657Cys	50.0/51.0	–	–	–	–
84	–	–	–	–	*CBL*	c.1096–110del643	p.Glu366_Phe488del	NA/NA	–	–	–	–
85	*PTPN11*	c.226G>A	p.Glu76Lys	47.5/4.4	–	–	–	–	–	–	–	–
86	*KRAS*	c.38G>A	p.Gly13Asp	38.9/3.1	–	–	–	–	–	–	–	–
89[c]	–	–	–	–	*PTPN11*	c.1502T>G	p.Ser502Ala	50.0/49.9	–	–	–	–
91[c]	–	–	–	–	*PTPN11*	c.218C>T	p.Thr73Ile	49.0/48.0	–	–	–	–
92[c]	–	–	–	–	–	–	–	–	–	–	–	–

NA, not available.
[a]Variant allele frequency (VAF) in tumor/reference samples, where the reference was CD3+ T cells, except for subject 63, for whom umbilical cord was used as the reference. [b]Substantial contamination of tumor cell components in the CD3+ T cell reference. [c]Noonan syndrome–associated myeloproliferative disorder.

translocations that result in an aberrant fusion gene (*NUP98-SETBP1*) and overexpression of *SETBP1* in T cell acute lymphoblastic leukemia (T-ALL) and acute myeloid leukemia (AML), respectively[12,13]. *SETBP1* is one of the downstream targets induced by the Evi-1 oncoprotein[14] and, together with *EVI1* and its homolog *PRDM16* (also known as *MEL1*), was reported to be activated through retrovirus integration. SETBP1 is also known to augment the recovery of granulopoiesis after gene therapies for chronic granulomatous disease[15]. *SETBP1* overexpression is found in more than 27% of adult AML cases and is associated with poor survival[13]. The discovery of recurrent hotspot mutations of *SETBP1* provides unequivocal evidence for the leukemogenic role of deregulated SETBP1 function. Notably, the *SETBP1* mutation encoding p.Asp868Asn was identical to one of the *de novo* mutations reported to be causative in Schinzel-Giedion syndrome (SGS; MIM 269150), which is a highly recognizable congenital disease characterized by severe mental retardation, distinctive facial features and

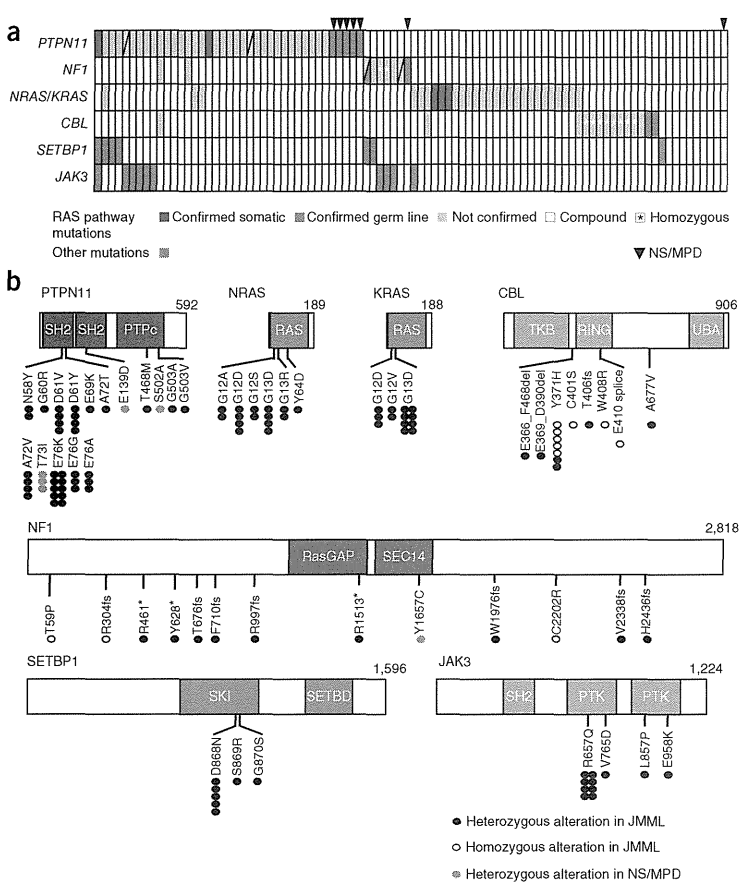

Figure 1 *Mutation profiles of 92 JMML cases.* (**a**) The mutation status of RAS pathway genes and 2 newly identified gene targets in a cohort of 92 JMML cases is summarized. NS/MPD, *Noonan syndrome–associated* myeloproliferative disorder. (**b**) The distribution of alterations is shown for each protein. SH2, Src homology 2 domain; PTPc, protein tyrosine phosphatase, catalytic domain; RAS, Ras GTPase family domain; TKB, tyrosine kinase–binding domain; RING, RING-finger domain; UBA, ubiquitin-associated domain; RasGAP, a region of similarity with the catalytic domain of the mammalian p120RasGAP protein in neurofibromin; SEC14, Sec14p-like lipid-binding domain; SKI, v-ski sarcoma viral oncogene homolog domain; SETBD, SET-binding domain; PTK, pseudokinase domain of the protein tyrosine kinases.

Table 2 Subject characteristics

Characteristic	Total cohort (n = 92)	Secondary mutations		P value
		Yes (n = 16)	No (n = 76)	
Sex (male/female)	61/31	12/4	49/27	NS
Median age at diagnosis in months (range)	19 (1–160)	38 (2–160)	13 (1–79)	<0.001
Diagnosis				
JMML	85	16	69	
NS/MPD	7	0	7	
Genetic mutations in RAS pathway				
PTPN11	39	9	30	NS
NF1	9	5	4	0.001
RAS (*NRAS* or *KRAS*)	28 (15/13)	2 (1/1)	26 (14/12)	0.08
CBL	14	0	14	0.06
Without RAS pathway mutation	10	1	9	NS
Secondary genetic mutations				
SETBP1	7	7	0	
JAK3	10	10	0	
Cytogenetics				
Normal karyotype	77	12	65	NS
Monosomy 7	8	1	7	NS
Trisomy 8	4	2	2	NS
Other abnormalities	3	1	2	NS
WBC count at diagnosis $\times 10^9$/l, median (range)	30.0 (1.0–563)	29.6 (5.6–563)	30.0 (1.0–131)	NS
Monocyte count at diagnosis $\times 10^9$/l, median (range)	4.6 (0.2–31.6)	3.1 (0.5–15.2)	4.9 (0.2–31.6)	NS
Percent HbF at diagnosis, median (range)	21 (0–68)	26 (9–55)	16 (0–68)	NS
PLT at diagnosis $\times 10^9$/l, median (range)	61.0 (1.4–483)	47.5 (1.4–175)	65.0 (5.0–483)	NS
HSCT (+/–)	56/36	16/0	40/36	
Alive/deceased	62/30	7/9	55/21	
Percent probability of 5-year overall survival (95% CI)	60 (46–71)	33 (10–59)	65 (49–77)	0.10
Percent probability of 5-year transplantation-free survival (95% CI)	15 (6–27)	0 (0–0)	18 (8–33)	0.007

JMML, juvenile myelomonocytic leukemia; NS/MPD, Noonan syndrome–associated myeloproliferative disorder; WBC, white blood cell; HbF, hemoglobin F; HSCT, hematopoietic stem cell transplantation; NS, not significant. We compared the difference between the subjects with and without secondary mutation, and P values were calculated by two-sided Fisher's exact test or Mann-Whitney U test.

multiple congenital malformations. Individuals with SGS with this mutation have a higher than normal prevalence of tumors, including of neuroepithelial neoplasia[16], although development of myeloid malignancies has not been reported so far.

To further validate our findings, we screened the entire cohort of 92 JMML cases for gene mutations in the newly identified 3 genes together with known RAS pathway targets using deep sequencing[17] (**Supplementary Fig. 5**).

RAS pathway mutations were found in 82 of 92 cases (89%) in a mutually exclusive manner, with *PTPN11* mutations predominant, followed by *NRAS*, *KRAS*, *CBL* and *NF1* mutations (**Fig. 1a** and **Table 2**). In accordance with previous reports, most of the *CBL* (8/14) and *NF1* (4/9) mutations were biallelic (**Fig. 1a,b** and **Supplementary Table 2**)[2,3,18], whereas the majority of mutations in *PTPN11*, *NRAS* and *KRAS* were heterozygous[4]. The individuals without RAS pathway mutations (n = 10) were vigorously investigated by whole-genome sequencing of tumor-normal paired samples (n = 2; **Supplementary Fig. 6**) or by whole-exome sequencing of only tumor samples (n = 8; **Supplementary Fig. 7**). As anticipated, we found no known RAS pathway mutations.

On the other hand, 18 mutations were found in *SETBP1* (n = 7) or *JAK3* (n = 11) in 16 cases (**Fig. 1a,b**, **Table 2** and **Supplementary Table 2**), with these mutations more frequent in cases with mutated *PTPN11* (and possibly *NF1*) than in cases with mutated *NRAS*, *KRAS*

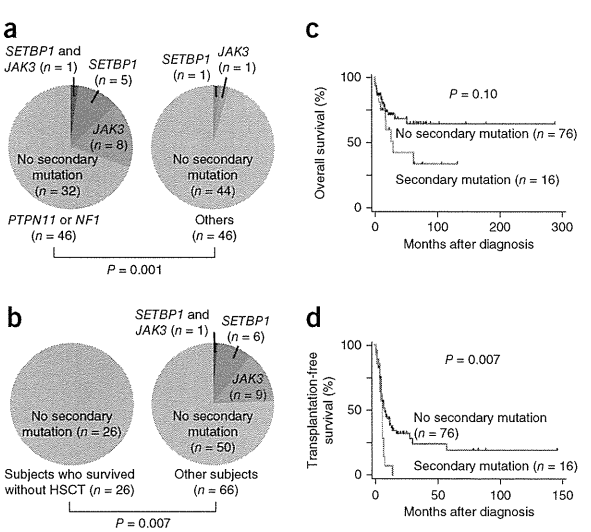

Figure 2 Clinical features of JMML cases with or without secondary mutations. (**a**,**b**) Frequency of secondary mutations in individuals with JMML depending on the type of RAS pathway mutations (left, *PTPN11* or *NF1*; right, other or no mutations) (**a**) and the status of HSCT (**b**). P values were calculated by two-sided Fisher's exact test. (**c**,**d**) The impact of secondary mutations on overall (**c**) and transplantation-free (**d**) survival is shown in Kaplan-Meier survival curves, where statistical significance was tested by log-rank test.